De la Cueva-Alique, I. et al. (2022) 'Stereoselective synthesis of oxime containing Pd() compounds: highly effective, selective and stereo-regulated cytotoxicity against carcinogenic PC-3 cells', Dalton transactions : an international journal of inorganic chemistry, 51(34), pp. 12812–12828.

Available at https://doi.org/10.1039/d2dt01403c

Journal Name

ARTICLE

Received 00th January 20xx,
Accepted 00th January 20xx

DOI: 10.1039/x0xx00000x

www.rsc.org/

Stereoselective synthesis of oxime containing Pd(II) compounds: Highly effective, selective and stereo-regulated cytotoxicity against carcinogenic PC-3 cells

Isabel de la Cueva-Alique,[a] Elena de la Torre-Rubio,[a] Laura Muñoz-Moreno,[b] Alicia Calvo-Jareño,[a] Adrián Pérez-Redondo,[a] Lourdes Gude,[a] Tomás Cuenca,[a] Eva Royo*[a]

New palladium compounds [Pd{(1*S*,4*R*)-NOH^NH(R)}Cl_2] (R = Ph **1a** or Bn **1b**), [Pd{(1*S*,4*R*)-NOH^NH(R)}{(1*S*,4*R*)-NO^NH(R)}][Cl] (R = Ph **2a** or Bn **2b**) and corresponding [Pd{(1*R*,4*S*)-NOH^NH(R)}Cl_2] (R = Ph **1a'** or Bn **1b'**) and [Pd{(1*R*,4*S*)-NOH^NH(R)}{(1*R*,4*S*)-NO^NH(R)}][Cl] (R = Ph **2a'** or Bn **2b'**) have been synthesized. Novel compounds **1a**, **1b**, **2b** (and **1a'**, **1b'**, **2b'**) were obtained in solution as a mixture of diastereomers whose relative ratios depend on the solvent and the nature of the amino substituent. In contrast, the synthetic reactions of derivatives **2a** and **2a'** were stereospecific, and afforded single enantiomers of absolute configuration (S_N,1S_C,4R_C)-(R_N,1S_C,4R_C) and (R_N,1R_C,4S_C)-(S_N,1R_C,4S_C), respectively. All compounds have been fully characterized by NMR and IR spectroscopy, time-dependent UV-spectroscopy, ESI-HR-MS in water, and CHN elemental analysis. Absolute configurations of major epimers of **1a** and **1a'**, both epimers of **1b** and enantiomer **2a'** were determined by single crystal X-ray crystallography, and endorsed by 2D NOESY NMR experiments in solution. Additionally, the pH-dependent stability of **2b** in water was assessed by ^{1}H-NMR spectroscopy. Metal derivatives have been tested *in vitro* against three human cancer (prostate PC-3, cervical HeLa, and breast MCF-7) cell lines. The highest anticancer activities were shown by palladium compound **2a'** in all cancer cells, with IC_{50} values up to 80 times lower than those found for cisplatin. The cytotoxicity of **2a** and **2a'** is stereo-dependent, with IC_{50} values that differ significantly for each enantiomer in all the cell lines tested. Cytotoxic activity of **2a** and **2a'** was further evaluated against the non-tumorigenic human prostate RWPE-1 cell line, revealing a selectivity index (SI) of ca. 30 for derivative **2a'**. DNA interactions have been investigated by equilibrium dialysis, Fluorescence Resonance Energy Transfer (FRET) DNA melting assays, and viscometric titrations, pointing to groove and/or external binding. Cell cycle assay on PC-3 cells after treatment with **2a** or **2a'** shows cell cycle arrest in the S and G2/M phases, especially when cells are treated with compound **2a'**.

Introduction

The design of platinum compounds with non-traditional structures emerged as a strategy to affect DNA differently from cisplatin (cis-diamminedichloroplatinum(II)), an approach that can be exploited to address systemic toxicity and resistance,[1–6] two of the main handicaps of cisplatin. Following this approach, a variety of "rule breaking" Pt(II) compounds (*trans*-, polynuclear, mono-functional and/or substitution inert Pt(II) complexes) have been prepared, and shown different cytotoxic profiles and DNA-binding properties than cisplatin analogues.[3,5–9]

For the last decade, Pd(II) compounds[10–17] have broadly been explored as alternatives to the currently used anticancer drug cisplatin, mainly due to their similar coordination geometry and chemistry. However, Pd(II) compounds are more labile and suffer from aquation and ligand-exchange rates much faster than Pt(II) analogues. It soon became apparent that a rationale choice of ligands was requisite to render Pd(II) compounds suitable as anticancer drugs. The use of chelating ligands, preferentially based on strongly coordinating atoms as P, N, S or C, and sterically demanding enough to protect the metal centre from rapid hydrolysis has produced highly valuable derivatives.[11,14,15,17] Padeliporfin (TOOKAD® soluble), a porphyrin-derived Pd(II) complex, was recently approved for clinical use by the European Medicines Agency as a potent vascular-targeted, photodynamic therapy agent for the treatment of localised prostate cancer.[18] Recent reviews on the subject demonstrate that several Pd(II) compounds with "rule-breaking" molecular structures, often display anticancer properties *in vitro* and *ex vivo* higher than Pt(II) counterparts or cisplatin, even towards tumours resistant to cisplatin and

[a] *Universidad de Alcalá, Instituto de Investigación Química "Andrés M. del Río" (IQAR), Departamento de Química Orgánica y Química Inorgánica, 28805 Alcalá de Henares, Madrid, Spain.*
[b] *Universidad de Alcalá, Facultad de Medicina y Ciencias de la Salud, Departamento de Biología de Sistemas, 28805 Alcalá de Henares, Madrid, Spain.*

†Electronic Supplementary Information (ESI) available: Representative NMR, UV-vis, HR-ESI-MS spectra, cell cycle assay, FRET-melting curves and X-ray data of compounds **1a-1**, **1a'-1**, **1b-1, 1b-2** and **2a'**. See DOI:

derivates.[15,17] From the existing data, it can be inferred that DNA interactions associated with most successful Pd(II) compounds are also distinct from that of classical Pt(II) derivatives.[10,11,13,15] Among those Pd(II) derivatives structurally different from cisplatin, a large majority contain potentially DNA intercalating ligands.[6,9,19–22]

On the other hand, the importance of stereochemistry on biological activity is well recognized in the anticancer metallodrug design.[23,24,33,34,25–32] As a part of an ongoing research project, we have used enantiopure amino-oxime pro-ligands derived from commercially available and low-cost natural terpenes[35,36] to prepare a variety of water-soluble, enantiopure Ru(II), Ti(IV), Pd(II) and Pt(II) compounds that have already demonstrated the great potential of this approach in the design of novel anticancer metallodrugs.[37–40] Other oxime metal compounds have also been reported to have interesting antitumor properties and different DNA interactions to that of cisplatin (see for example Pt,[41–47] Pd,[48–51] Rh, Ir,[52–54] and Ru[53,55–58]). Regarding Pd(II) coordination chemistry, oxime groups are excellent ligands for stabilization purposes, with a wide versatility of coordination modes going from mono-κN,[59] -κO[42] to di-hapto κ^{2}N,O either with *side on* or bridging coordination.[60–64] In addition, oxime derivatives have also shown advantageous biological activities for cancer treatment (i.e., inhibition of protein kinases, analgesic, anti-inflammatory and/or anticancer potential).[65–68]

We reported recently water-soluble, enantiopure, oxime-containing Pd(II) pincer compounds that effectively modulate adhesion and migration processes of cancer PC-3 cells.[64] Such metal complexes likely interact with double stranded (ds) DNA by a partial, non-classical intercalation and/or by groove binding. Thus, we become interested in the synthesis of chiral, Pd(II) *substitutionally-inert*[69] compounds with oxime, non-intercalating containing ligands, and their impact on their potential biological effects and DNA interactions. We report herein the synthesis and full characterization of novel chiral palladium derivatives containing one or two enantiopure N-based chelating amino-oxime ligands (Fig. 1).

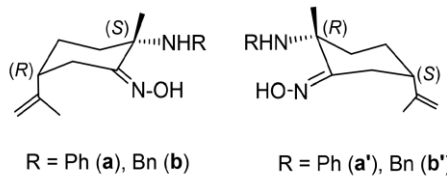

Fig.1. Optically active amino-oxime pro-ligands used in this report.[36]

The behaviour in water of the novel compounds was studied by UV-vis and/or ^{1}H-NMR spectroscopy. In addition, we have investigated the cytotoxic activity of the oxime-containing complexes against a variety of cell lines, as well as their DNA interactions. The effect of most cytotoxic derivatives on the cycle of PC-3 cells is also reported.

Synthesis and characterization of dichlorido metal compounds

In search of a synthetic general route to amino-oxime Pd(II) derivatives, $K_2[PdCl_4]$ or, alternatively, $[Pd(COD)Cl_2]$ (COD = 1,5-cyclooctadiene) was reacted with (1*S*,4*R*)-{NOH^NH(R)} (R = phenyl (Ph) **a**, or benzyl (Bn) **b**), in molar ratios [Pd]:[pro-ligand] of 1:1. The solids obtained from the reaction solutions show, in their ^{1}H NMR spectra in chloroform-d_1, the formation of a complicated set of resonances, which can be ascribed to at least three (from reaction with **a**) or four (from reaction with **b**) new Pd(II) compounds. The products are formed in solution together with the concomitant precipitation of corresponding ammonium oxime derivatives (1*S*,4*R*)-{NOH^NH(R)·HCl} (R = phenyl (Ph) **a·HCl** or benzyl (Bn) **b·HCl**), identified by ^{1}H NMR in DMSO-d_6.

To avoid dehydrochlorination processes assisted by the presence of the basic amino function contained in the pro-ligands, $[Pd(COD)Cl_2]$ was treated directly with the enantiopure ammonium salts **a·HCl** or **b·HCl** in dichloromethane. Under such acidic conditions, the reaction proceeds in ca. 24 h at room temperature with elimination of COD and HCl and formation of pure dichlorido Pd(II) compounds [Pd{(1*S*,4*R*)-NOH^NH(R)}Cl_2] (R = Ph **1a** or Bn **1b**) (Fig. 2).

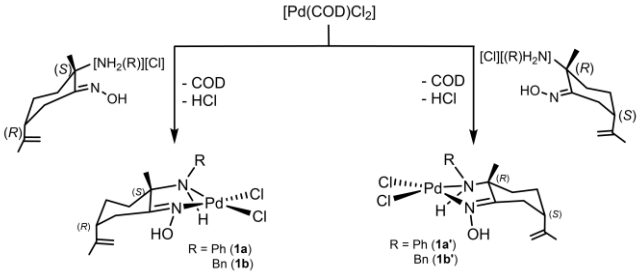

Fig. 2. Synthesis of novel dichlorido palladium compounds **1a**, **1b**, **1a'** and **1b'**.

Coordination of the amino unit to the metal gives rise to a new stereogenic centre at the nitrogen atom, resulting in the possible formation of two different diastereomers (epimers) of absolute configuration (S_N,1S_C,4R_C) and (R_N,1S_C,4R_C). The novel palladium dichlorido compounds have been characterized as a mixture of [Pd{(S_N,1*S*,4*R*)-NOH^NH(R)}Cl_2] (R = Ph **1a-1** or Bn **1b-1**) and [Pd{(R_N,1*S*,4*R*)-NOH^NH(R)}Cl_2] (R = Ph **1a-2** or Bn **1b-2**), detected by NMR spectroscopy (in chloroform-d_1 solution) in ca. 1:0.2 and 0.8:1 ratio, respectively. The configurational stability of these mixtures remains, in the chloroform-d_1 solutions tested, for at least 72 h and temperatures up to 60-70 °C.

Analogous treatment of $[Pd(COD)Cl_2]$ with enantiomers (1*R*,4*S*)-{NOH^NH(R)·HCl} (R = Ph **a'·HCl** or Bn **b'·HCl**) affords corresponding [Pd{(1*R*,4*S*)-NOH^NH(R)}Cl_2] (R = Ph **1a'** or Bn **1b'**), obtained as a mixture of the epimers [Pd{(R_N,1*R*,4*S*)-NOH^NH(R)}Cl_2] (R = Ph **1a'-1** or Bn **1b'-1**) and [Pd{(S_N,1*R*,4*S*)-NOH^NH(R)}Cl_2] (R = Ph **1a'-2** or Bn **1b'-2**), in ratios of ca. 1:0.2 or 0.8:1, respectively (Fig. 2).

CHN Elemental analysis of the solids **1a**, **1b** (or **1a'**, **1b'**) confirmed the same chemical composition for the epimers observed in solution, **1a-1** and **1a-2**, **1b-1** and **1b-2** (or **1a'-1** and **1a'-2**, **1b'-1** and **1b'-2**) and endorse their isomeric relationship.

Enantiomers **1a-1** and **1a'-1** can be isolated as pure solids by crystallization from the chloroform solution that contains them, whereas epimers **1b-1** and **1b-2** crystallize together, making their separation unfeasible by this technique. Suitable crystals obtained for all of them allowed determination of their absolute configuration by single-crystal X-Ray diffraction studies.

Enantiopure derivatives **1a-1**, **1a'-1** (Fig. 3, Table S1 ESI) and the epimeric mixture of **1b-1**, **1b-2** (Fig. 4, Table S2 ESI) show a square planar geometry around the Pd centre, where the metal is coordinated to both N atoms of amino and oxime functions. The most noticeable characteristic of their molecular structures is the presence of intramolecular hydrogen bonds =NOH···Cl-Pd, with O···Cl distances of 3.182(6) Å (**1a-1**), 3.179(6) Å (**1a'-1**), 3.086(7) Å (**1b-1**) and 2.999(7) Å (**1b-2**). Such short intramolecular contacts have also been found in other oxime Pd(II) and Pt(II) dichlorido compounds.[43,70–72]

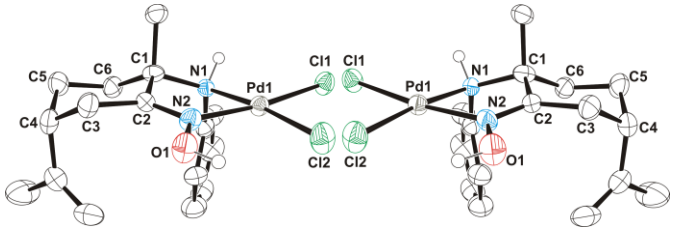

Fig. 3. ORTEP drawing of compounds **1a-1** (LEFT) and **1a'-1** (RIGHT) with 50% probability ellipsoids. Hydrogens bonded to carbon atoms have been omitted for clarity. Representative lengths (Å) and angles (deg) of **1a-1**: Pd(1)-N(1) 2.048(5); Pd(1)-N(2) 1.992(6); Pd(1)-Cl(1) 2.274(2); Pd(1)-Cl(2) 2.294(2); N(2)-O(1) 1.378(7); N(1)-Pd(1)-N(2) 81.3(2); N(1)-Pd(1)-Cl(1) 92.0(2); N(2)-Pd(1)-Cl(2) 94.0(2); Cl(1)-Pd(1)-Cl(2) 92.9(1).

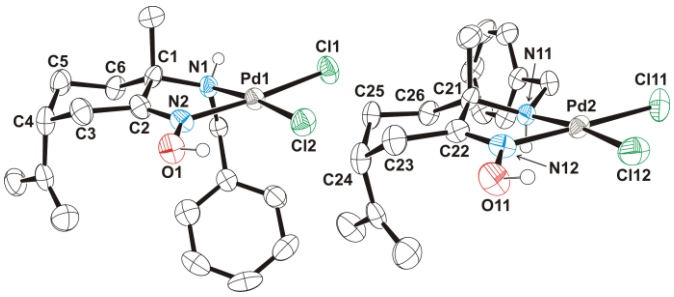

Fig. 4. ORTEP drawing of compounds **1b-1** (LEFT), **1b-2** (RIGHT) with 50% probability ellipsoids. Hydrogens bonded to carbon atoms have been omitted for clarity. Representative lengths (Å) and angles (deg) of **1b-1**: Pd(1)-N(1) 2.049(7); Pd(1)-N(2) 1.996(7); Pd(1)-Cl(1) 2.297(2); Pd(1)-Cl(2) 2.293(2); N(2)-O(1) 1.371(8); N(1)-Pd(1)-N(2) 80.7(3); N(1)-Pd(1)-Cl(1) 92.7(2); N(2)-Pd(1)-Cl(2) 91.9(2); Cl(1)-Pd(1)-Cl(2) 94.8(1).

In light of the X-ray structures, it becomes clear that the observed stereoselectivity is directed, apart from other considerations,[73,74] by the nature of the aromatic substituent at the amino N. Accordingly, the preferred N configuration of the major epimers **1a-1** or **1a'-1** avoids NH**Ph** and NCq**Me** contacts, while the more flexible benzyl allows S_N or R_N configurations almost indistinctly, to produce mixtures of **1b-1** + **1b-2** in a ca. equimolar ratio.

When the enantiopure crystalline solid **1a-1** (or **1a'-1**) is re-dissolved in chloroform-d_1 at room temperature, epimerization[75–77] affords, after the first 30 min, a mixture of **1a-1** + **1a-2** (or **1a'-1** + **1a'-2**) in a 1:0.2 ratio, which then remained constant for the next 48 h.

The different relative intensity of each set of resonances found in the NMR spectra of **1a** and **1b**, helped us to perform full NMR spectroscopy characterization of each epimer, with the help of bidimensional ^{1}H–^{1}H COSY, ^{1}H–^{1}H NOESY, ^{13}C–^{1}H HSQC, HMBC and ^{15}N–^{1}H HMBC experiments. As expected for enantiomer pairs, analytical and spectroscopic data of **1a** or **1b** are identical to those observed for **1a'** or **1b'**, respectively (see Experimental Section and ESI, Figs. S7-S22).

Variation in chemical shifts of the nitrogen signals arising from the oxime and amino groups in **1a** (δ 262.4 and 62.1 **1a-1**, ^{15}N resonances of minor **1a-2** are not detected) or **1b** (δ 255.3 and 50.9 **1b-1**, 264.2 and 50.9 **1b-2**), compared to those found in **a** (δ 343.5 and 84.1) or **b** (δ 340.0 and 60.0), respectively, agrees well with a κ^{2}N bidentate coordination of the ligands in the novel Pd(II) compounds. The chemical shift of the signals due to proton and carbon atoms closest to coordinated N atoms compared to those detected for the same fragments in the NMR spectra of metal-free amino-oxime derivatives also changed the most. Thus, ^{1}H NMR NO**H**, N**H** signals (δ 9.93, 5.59 **1a-1**, 10.07, 6.68 **1a-2**, 9.80, 4.89 **1b-1**, 9.99, 5.47 **1b-2**), and ^{13}C resonances due to **C**q=NOH, **C**qNH (δ 170.5, 73.5 **1a-1**, 169.0, 72.4 **1a-2**, 170.3, 71.4 **1b-1**, 169.1, 71.8 **1b-2**), are downfield shifted relative to those found in pro-ligands **a** (δ 8.41, 3.57 and 164.9, 57.0) or **b** (δ 9.40, 1.19 and 163.0, 57.0), respectively.

The absolute configuration of the amino nitrogen confirmed by X-Ray molecular structures is endorsed by 2D NOESY experiments in solution. 2D NOESY spectra revealed the association of the N**H** amino proton signal of **1a-1** and **1b-1** (or **1a'-1** and **1b'-1**) with the resonance due to CqNC**H$_3$** fragments (δ 6.70 and 2.25 **1a-1**, **1a-1'**, δ 4.87 and 2.04 **1b-1**, **1b'-1**) (Fig. 5 LEFT and Fig. S15 ESI). Epimers **1b-2**, **1b'-2** show, instead, NOESY contacts between N**H** and C**H$_2$**(6) resonances at δ 5.47 and 1.63, respectively (see Fig. 5 RIGHT and Fig. S22 ESI).

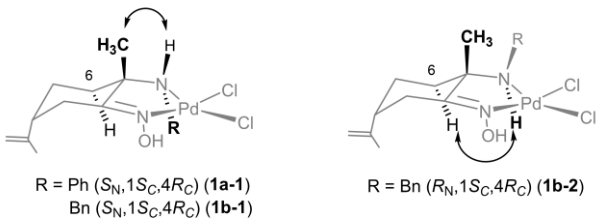

R = Ph (S_N,1S_C,4R_C) (**1a-1**)
Bn (S_N,1S_C,4R_C) (**1b-1**)

R = Bn (R_N,1S_C,4R_C) (**1b-2**)

Fig. 5. Associated proton resonances detected in the 2D NOESY spectra of epimers **1a-1, 1b-1** (LEFT) and **1b-2** (RIGHT).

Synthesis and characterization of "*substitutionally inert*" Pd(II) compounds

We were especially interested in the synthesis and biological study of palladium compounds lacking labile chloride ligands. Taking into account our initial experimental results obtained from the reaction of [Pd(COD)Cl$_2$] and **a** or **b**, the reaction was performed in the presence of an external base as NEt$_3$, in molar

ratios [Pd]:[proligand]:[base] of 1:2:2. Under these conditions, $[NHEt_3]Cl$ and pure cationic compounds [Pd{(1*S*,4*R*)-NOH^NH(R)}{(1*S*,4*R*)-NO^NH(R)}][Cl] (R = Ph **2a** or Bn **2b**) formed. Structural data of the metallic compounds confirm the presence of mixed amino-oxime and deprotonated amino-oximato ligands (Fig. 6). A greater excess of NEt_3 ([Pd]:[proligand]:[base] up to 1:2:8) leads to the same results. Analogous experimental procedure starting from $[Pd(COD)Cl_2]$ and **a'** or **b'** affords corresponding [Pd{(1*R*,4*S*)-NOH^NH(R)-κ²N}{(1*R*,4*S*)-NO^NH(R)-κ²N}][Cl] (R = Ph **2a'** or Bn **2b'**) (Fig. 6).

Fig. 6. Synthesis of compounds **2a**, **2b**, **2a'** and **2b'**.

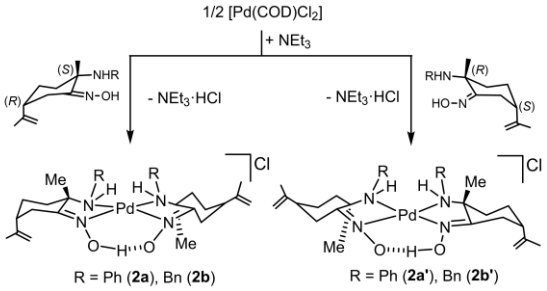

Once again, amino N coordination to palladium centre can produce different diastereoisomers, now of absolute configuration (S_N,1S_C,4R_C)-(S_N,1S_C,4R_C), (R_N,1S_C,4R_C)-(R_N,1S_C,4R_C) (both belonging to C_2 symmetry group) and (S_N,1S_C,4R_C)-(R_N,1S_C,4R_C) (C_1 symmetry) (Fig. 7). ^1H, ^{13}C and ^{15}N NMR spectra (chloroform-d_1) of **2a** (or **2a'**) showed the presence of only one stereoisomer solution of C_1 symmetry (Fig. S23-S29, ESI). In contrast, NMR spectra of **2b** show a mixture of two sets of resonances in a 1:0.3 ratio: one major set corresponds to a compound in the C_2 point group (**2b-1**) and one minor is attributable to a C_1 symmetric system (**2b-2**) (Fig. S30 and S33, ESI). The ratio keeps unaltered in the chloroform-d_1 solutions studied during at least 72 h and temperatures up to 80 °C.

Absolute configuration of **2a'**, namely (R_N,1R_C,4S_C)-(S_N,1R_C,4S_C), was confirmed through single-crystal X-Ray structure determination (Fig. 8, Table S3). The solid-state structure shows a square planar geometry around the Pd center, where the metal is coordinated to both ligands through N atoms of amino, oxime and oximato functions. Oxime and oximato are joint together by a =NO-H-ON= bond, forming a bridge where the hydrogen atom places closer to one of the oxygen, with bond distances O(1)-H(1) = 1.08(5) Å and O(2)···H(1) = 1.36(6) Å. This structural feature distinguishes the compound from others oxime oximato Pd(II) derivatives found in the literature, where O-H-O bond distances are equal and the atoms PdN_2O_2H are coplanar.[78] Another notable feature of the molecular structure of **2a'** is the π-π contacts found between phenyl rings, with a distance between centroids of 3.61 Å and an angle between phenyl planes of 8°. Most likely, this weak interaction plays an important role in the observed stereospecific formation of the compound.

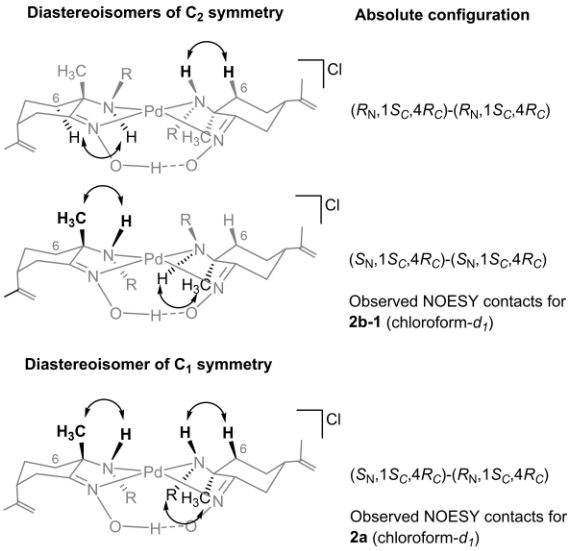

Fig. 7. Possible diastereomers of **2a**, **2b** and associated proton resonances detected in the 2D NOESY spectra.

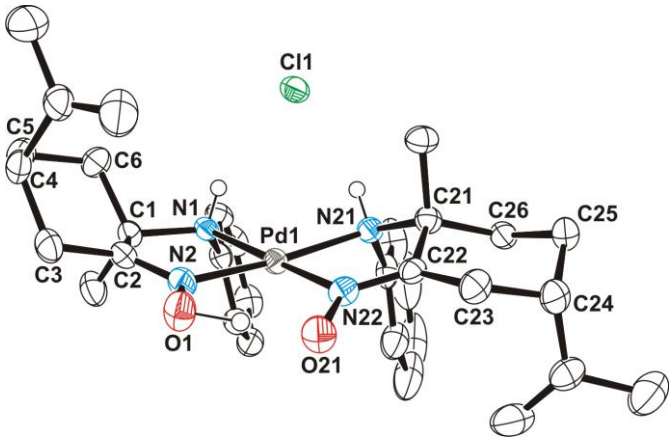

Fig. 8. ORTEP drawing of compound **2a'** with 50% probability ellipsoids. Hydrogens bonded to carbon atoms have been omitted for clarity. Representative lengths (Å) and angles (deg): Pd(1)-N(1) 2.077(3); Pd(1)-N(2) 1.973(3); Pd(1)-N(21) 2.080(3); Pd(1)-N(22) 1.976(3); N(2)-O(1) 1.355(4); N(22)-O(21) 1.343(4); N(1)-Pd(1)-N(2) 81.4(1); N(21)-Pd(1)-N(22) 81.1(1); N(1)-Pd(1)-N(21) 101.2(1); N(2)-Pd(1)-N(22) 95.9(1).

Oxime and amino hydrogen atoms appear in the ^1H NMR spectrum of **2a** and **2b-2** (or **2a'** and **2b'-2**) as three resonances of relative intensities 1:1:1. Instead, the C_2 symmetric major epimer, **2b-1**, shows only two signals ascribed to NO**H** and N**H** atoms of relative intensities 1:2 (see Experimental and Fig. S30). Chemical shifts of the ^{13}C NMR signals due to **C**q=NOH and **C**qNH and ^{15}N NMR of =**N** and –**N**HPh also confirm, for compounds **2a** and **2b** (or **2a'** and **2b'**) the coordination in solution of both ligands through =**N** and -**N**HPh atoms.

Calculated data of specific optical rotation in chloroform solution for **2a** and **2a'** ($[\alpha]^{23}_D$ (deg·dm^{-1}·dL·g^{-1}) = +10.33 ± 1.3 **2a**, -10.33 ± 1.3 **2a'**) evidence the enantiomeric relationship of both diastereoisomers.

In addition, the compounds were investigated by 2D NOESY spectroscopy (see Fig. 7). Spectra of **2a** and **2a'** (C_1 symmetry

enantiomers) show the association of the N**H** signals (at δ 8.77 and 8.52) with those of C**H₂**(6) and C**H₃**CqN (δ 2.79, 1.06 and 2.02, respectively). Also, contacts between aromatic hydrogens at δ 7.09 (Ph) and 1.00 (C**H₃**CqN 1) are apparent (Fig. 7 and Fig. S29, ESI). For the C_2 symmetric major epimer of **2b**, **2b-1**, (or of **2b'**, **2b'-1**) the spectrum shows NOESY contacts between N**H** and C**H₃**CqN resonances, detected at δ 5.90 and 1.14, pointing to an absolute configuration (S_N,1S_C,4R_C)-(S_N,1S_C,4R_C), (Fig. 7 and S37). The low intensity of the signals due to minor **2b-2** (or **2b'-2**), prevents detection of NOESY contacts. However, the set of NMR signals can only be due to a C_1 symmetric compound, for which only configuration (S_N,1S_C,4R_C)-(S_N,1S_C,4R_C), (or (R_N,1R_C,4S_C)-(R_N,1R_C,4S_C) for corresponding enantiomer **2b'-2**) is possible (Fig. 7).

As observed before for dichlorido derivatives **1a** or **1b** (**1a', 1b'**), preventing -NH**R** and -NCq**Me** contacts seems crucial for the observed diastereoselectivity in chloroform solution, and the substituents nature at the amino group is, again, determining. Thus, sterically demanding benzyl groups of **2b** do not allow major formation of the C_1 symmetric epimer, while for **2a** this is the only epimer formed.

On the other hand, the reaction of **2b** with KPF_6 in dichloromethane affords an orange solid, whose ^{19}F and ^{31}P NMR spectra confirm the presence of the counteranion $[PF_6]^-$ and the cationic character of **2b** (See Experimental Part). Elemental CHN analysis of **2a** and **2b** (or **2a'** and **2b'**) also validates the proposed molecular structures.

Regarding IR spectroscopy, amino-oxime pro-ligands **a** or **b** exhibit strong, broad ν(OH/NH) bands at ῡ 3100/3320 cm^{-1} and C=N stretching frequencies at ῡ 1644 cm^{-1}. Palladium novel compounds show absorptions at ῡ 3389, 3494 and 1637 (**1a**, **1a'**), 3279, 3504 and 1641 (**1b**, **1b'**), 3385, 3642 and 1641 (**2b**, **2b'**) and 3298, 3433 and 1599 cm^{-1} (**2a**, **2a'**), assigned to ν(OH/NH) bands and C=N stretching frequencies.

Behaviour of novel palladium compounds in water

We assessed the stability of complexes **1a**, **1b**, **2a**, and **2b** in water or PBS (phosphate buffered saline) solution by UV‑Vis spectroscopy. UV-Vis spectra of **1a** show shoulders at 244 and 293 nm, while no absorptions are discernable for **1b**. For derivatives **2a** and **2b**, bands at 246, 291, and 248 nm, respectively, are detected, all assignable to ligand to metal charge transfer (LMCT) bands by comparison with UV-vis spectra of corresponding free ligands **a** or **b**. None of the compounds shows significant changes in their UV‑vis spectrum over 72 h (ESI, Fig. S47-50).

Solubility in water of compounds **1a** (s = 0.87 ± 0.4 mM), **1b** (s = 1.37 ± 0.3 mM) and **2a** (s = 0.5 ± 0.1 mM) is sufficient to perform biological studies without the addition of DMSO, but do not allow detection of NMR resonances in water-d_2. Only **2b**, with a solubility of 5.8 ± 0.3 mM allows a time and pH-dependent ^1H NMR study.

Upon dissolution in water-d_2 (5.0 mM, pH = 7.3), ^1H NMR spectrum of **2b** (or **2b'**) showed two sets of resonances ascribed to **2b-1** and **2b-2** epimers (or **2b'-1** and **2b'-2**), with relative intensities 0.1:1. In contrast to that observed in chloroform-d_1, the major set of signals corresponds now to an epimer in the C_1 point group (**2b-2**), while the minor one is ascribable to a C_2 symmetric isomer (**2b-1**). This experimental result points to an epimerization process, leading to a different epimer ratio in water than observed in chloroform solution. Epimerization (or racemization) of metal coordinated stereogenic N atoms implies cleavage of M–N bond and subsequent intramolecular rearrangement.[75–77] Thus, the activation barrier of the process is highly dependent on the donor ability of the reaction solvent and the nature of the metal and the substituents at the chiral amino function, which determines the M-N bond strength.[74,79–81] For example, configurational stability of Ni(II) or Pd(II)-coordinated nitrogen has been reported to decrease substantially with the increasing coordinating ability of the reaction solvent.[74]

The ratio between both sets of signals is maintained during the following 96 h at 40 °C (Fig. S38, ESI). ^{13}C and/or ^{15}N NMR characterization of the mixture of **2b-1**+**2b-2** in water-d_2 evidence that coordination of the ligands through amino and oxime/oximato N atoms in both stereoisomers remains intact (Fig. S41-43). Furthermore, high-resolution electrospray ionization mass spectrometry (HR-ESI-MS) of the water solution after 72 h confirmed the molecular formula of the epimers, showing the main peak with the adequate isotopic pattern for $[M\text{-}Cl]^+$ at m/z = 649.2749 (100 %) (Fig. S58 ESI). Analogous behaviour is observed when **2b** (or **2b'**) is dissolved in methanol-d_4 (Fig. S44-46, ESI).

pH dependence of 2b in water

The initial sets of resonances observed in water suffered no apparent changes in the following 96 h within the 2.0-12.0 pH interval. Instead, acidification of water-d_2 solutions of **2b-1**+**2b-2** with DCl to pH* ≤ 2.0 caused the precipitation of a white-yellowish solid, identified (after evaporation and addition of chloroform-d_1 or DMSO-d_6) as a mixture of **1b** and **b·HCl**. The process is reversible, and the mixture of **1b** and **b·HCl** evolves to **2b-1**+**2b-2** when the solution is basified with NaOD to pH* > 2.0.

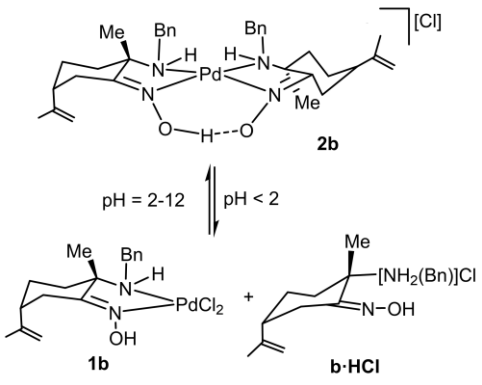

Fig. 9. Observed pH-dependent evolution of **2b** in water-d_2

This pH-dependent evolution is also critical in the synthesis of pure **1a**, **1b**, **2a**, or **2b**. Thus, treatment of $[Pd(COD)Cl_2]$ with **a** or **b** in molar ratios of 1:1 or 1:2 affords a mixture of **1a**, **2a** and **a·HCl** or **1b**, **2b** and **b·HCl**, respectively. Synthesis of pure **1a** or

1b was only practicable in acidic media (as that reached by the addition of ammonium salts **a·HCl** or **b·HCl** instead of free pro-ligands), while only the addition of external bases led to pure **2a** or **2b**.

Although the fate of **2a** (or **2a'**) in water could not be monitored by ^{1}H NMR, their water solutions were analysed by HR-ESI-MS after 72 h. The samples afforded a molecular peak with the correct isotopic pattern for $[M\text{-}Cl]^+$ at m/z = 621.2419, 100 % **2a** (or 621.2431, 100%, **2a'**) (ESI, Fig. S52, S53). These results confirm that the chemical composition of **2a** in aqueous media keeps unaltered, which agrees well with the time-dependent UV-vis study in water or PBS.

Lipophilicity

The partition coefficient between water and *n*-octanol (logP) is one of the most commonly used parameters that allows quantifying and optimizing drug-like pharmacokinetic properties.[82–87] We measure the *n*-octanol/water partition coefficient of derivatives **1a**, **1b**, **2a**, and **2b** by using the shake-flask method[84,88] at room temperature. Unfortunately, long dispersion data were obtained in repeated experiments for compounds **1a**, **1b**, and **2b**, most probably due to the different solubility of diastereomeric components of the mixtures, which prevented an accurate determination of their logP. This issue was not observed for **2a**, where the calculated value (logPo/w = +0.599 ± 0.05) is indicative of a low hydrophilic compound, more lipophilic than the clinical metallodrug cisplatin (log P = -2.27).[86,87]

***In vitro* cell studies**

The cytotoxic activity of derivatives **a·HCl**, **b·HCl**, **a'·HCl**, **b'·HCl**, cisplatin, and novel palladium compounds was assessed in human cervical carcinoma HeLa, breast and prostate adenocarcinoma MCF-7 and PC-3 cell lines. Most active palladium derivatives **2a**, **2a'** were also screened for their antiproliferative effects on the non-tumorigenic human prostate RWPE-1 cell line, and their mechanism of action was investigated by means of the cell cycle arrest assay.

Anti-proliferative studies

The *in vitro* effect of the compounds on cytotoxicity was tested by monitoring their ability to inhibit cell growth using the MTT assay and assessed through the determination of IC_{50} values after 72 h of treatment. The results are summarized in Table 1. Under these conditions, pro-ligands **a·HCl**, **b·HCl**, **a'·HCl**, **b'·HCl** are poorly cytotoxic in all tested cell lines (IC_{50} > 100 μM). Dichlorido palladium compounds **1a**, **1b** and corresponding **1a'**, **1b'** are moderately cytotoxic in the cell lines assessed, but with IC_{50} values 2-9 times higher than those found for cisplatin. The results obtained for compounds containing (1*S*,4*R*)- (namely **1a**, **1b**) or (1*R*,4*S*)-amino oxime ligands (**1a'**, **1b'**) are comparable, with no significant differences between them.

Table 1. IC_{50} values (μM) of **1a**, **1b**, **2a**, **2b** and corresponding **1a'**, **1b'**, **2a'**, **2b'** and cisplatin in human cervical carcinoma HeLa, breast adenocarcinoma MCF-7 and prostate cancer PC-3 cell lines.

Compound	HeLa	PC-3	MCF-7
1a	30.9 ± 0.7	28.0 ± 0.8	50.4 ± 3.7
1a'	38.8 ± 3.1	24.4 ± 0.3	53.8 ± 4.0
1b	49.2 ± 10.1	> 100	89.5 ± 5.9
1b'	60.8 ± 0.9	> 100	76.0 ± 0.2
2a	7.2 ± 0.48	0.79 ± 0.084	6.05 ± 1.3
2a'	1.71 ± 0.32	0.17 ± 0.048	4.92 ± 0.91
2b	12.8 ± 0.31	4.02 ± 0.44	9.02 ± 2.7
2b'	12.5 ± 2.2	5.16 ± 0.12	9.08 ± 0.55
cisplatin	11.8 ± 4.2	14.5 ± 2.5	9.8 ± 0.96

In contrast, amino oxime oximato Pd(II) derivatives are highly cytotoxic, with IC_{50} values that are better (or similar, see **2b** and **2b'** in HeLa or MCF-7 cells) than those of cisplatin. The most active compound in all evaluated cell lines is **2a'**, with calculated IC_{50} values from 1.5 up to 80 times lower than those found in cisplatin. Comparison of the effect of **2a** and **2a'** on HeLa and PC-3 cancer cells shows stereo-recognition, **2a'** being ca. 4 times more cytotoxic than **2a**. Several chiral palladium(II) derivatives with antitumor effects have been reported,[89–96] but only a few include a biological comparison of enantio- or diastereoisomers.[64,94–96] One of the most potent *in vitro* anticancer agent among them is *trans*-[1-menthyl-4-ethyl-1,2,4-triazol-5-ylidene]$_2$Pd(OCOCF$_3$)$_2$ (IC_{50} = 0.5-0.7 μM in MCF-7 and 2.3-2.6 μM in HeLa[96]), their two enantiomers showing nearly equal activity. Stereo-regulation of cytotoxicity was neither observed by us in enantiomeric pairs of monofunctional Pd(II) N,N,N pincer compounds[64] nor by Kordestani et al. in bis-chelating carboxamide Pd(II) enantiomers.[94] To the best of our knowledge, the chirality influence of Pd(II) compounds on cytotoxicity has only been reported before in 1,2-bis-(1H-benzimidazol-2-yl)-1,2-ethanediol containing Pd(II) enantiomers, (Λ)- being 2 times less active than the (Δ)-enantiomer in the MDA-MB231 and OVCAR-8 cell lines.[95]

In order to assess the selectivity of the cytotoxic effects of **2a** and **2a'** for cancerous cells, the compounds were also screened against the non-tumorigenic prostate cell line RWPE-1 (Table 2).

Table 2. IC_{50} values (μM) of **2a**, **2a'** and cisplatin in human prostatic cancer PC-3 and non-tumorigenic RWPE-1 cell lines.

Compound	PC-3	RWPE-1	SI
2a	0.79 ± 0.084	1.93 ± 1.0	2.4
2a'	0.17 ± 0.048	5.03 ± 0.74	29.6
cisplatin	14.5 ± 2.5	19.9 ± 1.1	1.4

Both derivatives are more toxic to PC-3 than to RWPE-1 cells, especially **2a'**, with a selectivity index (SI = IC_{50} (RWPE-1)/IC_{50} (PC-3)) close to 30. In contrast, cisplatin shows comparable activity in both prostate cell lines.

A variety of palladium "rule-breakers" compounds has shown higher in vitro antitumor activity than their Pt(II) counterparts or cisplatin.[14,15,105,97–104] IC_{50} values of compound **2a'** are within the range of other highly cytotoxic Pd(II) compounds described so far. For example, our derivative is ca. 55 times more cytotoxic

in prostatic cancer PC-3 cells than the promising [Pd(sac)(terpy)](sac)·4H_2O (sac = saccharinate, terpy = 2,2':6',2''-terpyridine), which has shown significant antitumor effects on Balb/c mice *in vivo*, and inhibit cell growth *in vitro* with IC_{50} values of 9.6 μM in PC-3 and 3.05 μM in MCF-7.[106,107] Other notable examples in the literature are the thiosemicarbazone containing compound [Pd(Ac4Et)$_2$] (Ac4Et = 2-acetyl pyridine 4N-ethyl thiosemicarbazone, IC_{50} = 0.14 μM, in MCF-7[100]), some monofunctional Pd(II) derivatives with N,N,S pincer ligands (IC_{50} within the range 2.6-28 μM in PC-3 and 6.4-70.0 μM in MCF-7[99,108]) and a variety of cyclopalladated complexes with N-heterocyclic carbenes (IC_{50} within the range 0.4-1.8 μM in Hela and active against Hela xenografts mice *in vivo*[100]).

DNA interaction studies

Traditionally, double stranded (ds) DNA has been considered one of the main cellular targets of platinum-based drugs. Structurally, the highly cytotoxic novel compounds **2a**, **2a'**, **2b** or **2b'** belong to the so called "rule breakers",[6,19,69,109] as they do not adjust to the conventional anticancer group 10 metal compounds. Taking into consideration the interesting results of biological activity displayed by **2a**, **2a'**, **2b** or **2b'**, exploring their potential DNA interactions was highly relevant, and thus, several assays testing their DNA recognition were carried out. Equilibrium dialysis, fluorescence-based DNA melting experiments and DNA viscosity titrations with ds DNA were used with this aim.

Equilibrium Dialysis experiments with Calf Thymus (CT) DNA were carried out to determine whether **2a**, **2a'**, **2b** or **2b'**, can bind ds CT DNA and to establish their binding affinity. In these assays, metal complexes were incubated with ds CT DNA at room temperature for 24 hours, after which the amount of compound bound to DNA was quantitated. Experiments were carried out using a protocol described by Chaires,[110] with some minor modifications (Experimental section). The results obtained are summarized in Table 3.

Table 3. DNA apparent association constants of compounds **2a**, **2a'**, **2b**, **2b'** obtained by equilibrium dialysis.[a]

Compound	2a	2a'	2b	2b'
Kapp (M^{-1}) x 10^{-4}	3.27 ± 0.37	3.42 ± 0.14	2.73 ± 0.81	3.49 ± 0.76

[a] Apparent association constants were calculated according to the equation $K_{app} = C_b/(C_f)(S_{total}-C_b)$, where C_b is the amount of metal complex bound, C_f is the free metal complex concentration and S_{total} = 75 μM, in monomeric units (bp).

Table 3 shows that the metal complexes **2a**, **2a'**, **2b** and **2b'** bind CT DNA with moderate affinity, with apparent binding constants in the order of 10^4 M^{-1}, and with no significant differences among the tested compounds.

Another aspect that deserves investigation is determining whether the metal complexes exert an effect on the DNA denaturing temperature (Tm). If the metal complex binds to DNA affecting the stability of the double helix, changes in the value of DNA Tm are commonly observed. Stabilization of duplex DNA via an intercalation mechanism usually results in increased values of Tm, while binding through recognition of the minor groove or external electrostatic-based interactions do not affect Tm values.

Variable-temperature (DNA FRET-melting) assays employing fluorescence-labelled short DNA oligonucleotides were carried out.[111] The sequence of choice was a 10-bp oligonucleotide designated as F10T labelled with two fluorophores, FAM at the 5' end and TAMRA at the 3' end.[112] Besides the metal complexes **2a**, **2a'**, **2b** or **2b'**, precursor ligands **a**, **b** and **a'**, **b'** were also included in this assay.

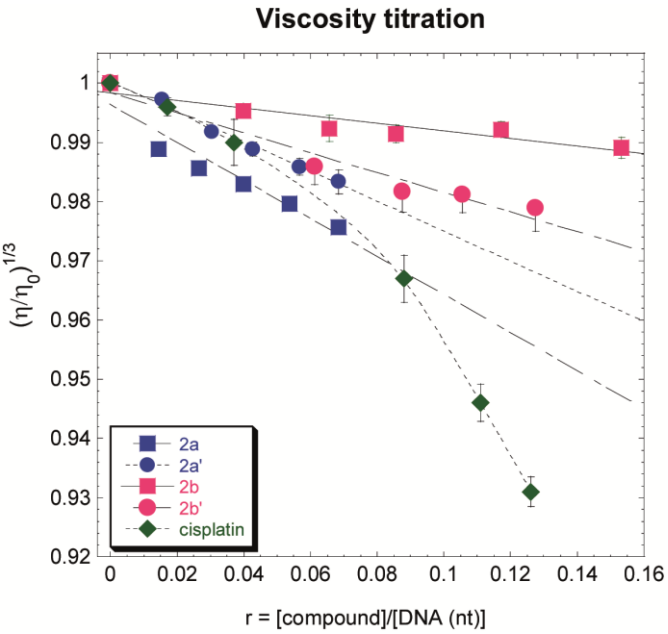

Fig. 10. Viscometric titrations of *Calf Thymus* (CT) DNA and metal complexes **2a**, **2a'**, **2b** and **2b'**, at 25 °C (10 mM sodium phosphate buffer, pH 7.2). Cisplatin is included for comparison.

All compounds were tested using a wide range of concentrations, from 1 μM to 10 μM. Under these experimental conditions, neither the metal complexes nor the ligand precursors affected dsDNA melting temperature (see representative example in Fig. S54, ESI). This is consistent with a non-intercalative mode of interaction with DNA and points to groove and/or external electrostatic binding.

In addition, DNA viscosity titrations were carried out to confirm the previous findings and to establish the nature of DNA interactions of **2a**, **2a'**, **2b**, and **2b'**. The measurement of DNA viscosity provides a simple and fast way to differentiate binding modes of DNA ligands (particularly non-covalent interactions, such as intercalation between base pairs *versus* groove or external binding).[113] Gradual titration of a DNA solution with increasing concentration of potential ligands, followed by the representation of the cubed root of the relative DNA viscosity $(\eta/\eta_o)^{1/3}$ versus the molar ratio of bound ligand to DNA nucleotide (r), allows the determination of a slope value that is correlated with the type of DNA binding mode.[114] Thus, groove binding compounds usually display a slope close to 0.0 (ca. in

the range -0.3 to 0.2), whereas classical mono-intercalants show a slope value close to 1.0.[113–115]

In the present study, metal complexes **2a**, **2a'**, **2b**, and **2b'** showed a linear $(\eta/\eta_o)^{1/3}$ versus r correlation in the compound to DNA ratios used in the experiments, and resulted in a slight decrease in DNA viscosity at increasing concentrations, with negative slope values of -0.32, -0.25, -0.07 and -0.17, respectively (Fig. 10). This decrease is reminiscent of the effect observed with other metallodrugs, such as cisplatin, which covalently binds to DNA, but is significantly lower.

As expected, and in good agreement with the results from the DNA melting experiments, viscosity titrations confirm that a classical intercalating interaction by metal derivatives **2a**, **2a'**, **2b**, and **2b'** can be ruled out. The viscosity slope values obtained fall within the experimental values reported for groove binding ligands, but the negative slope may also be compatible with a slight bending of the DNA double helix, especially in the case of compounds **2a**, **2a'**, which are the metal derivatives with a better profile, in terms of cytotoxic activity. Overall, these compounds are slightly decreasing DNA contour length and its viscosity in solution. It is known that metal complexes can bind DNA by partial or non-classical intercalation, decreasing the DNA contour length by bending or kinking the DNA helix.[116–118]

Effect of 2a and 2a' on the cell cycle of PC-3 cells

Based on the inhibitory effect on cell proliferation of complexes **2a** and **2a'**, their effect on the cell cycle of PC-3 cells was evaluated by flow cytometry at their IC_{50} concentration for 48 h. Cisplatin was included in the assay as a positive control. After treatment with **2a** or **2a'**, there was a significant increase of cells in the S-phase (6.26% **2a**, 8.57% **2a'** relative to control cells, ESI, Fig. S55) and a notable increase in the G2/M phase, especially for cells treated with **2a'** (8.71% **2a** and 16.77% **2a'** versus untreated cells). The effect is observed together with a decrease in cell population in the G1 phase (of 15.05 % **2a** and 25.65 % **2a'** versus untreated cells) and reveals a cell cycle arrest at the S and G2/M phases. Compared with cisplatin, compounds **2a** and **2a'** affect less the distribution of cells in the S-phase. This result agrees well with the study of their interactions with DNA that shows weaker structural damage on the nucleic acid relative to those caused by cisplatin.

Conclusions

We have developed a general route to novel chiral amino-oxime containing Pd(II) compounds from low-cost, enantiopure amino oxime derivatives. Appropriate modulation of the acidity-basicity reaction medium enables the chemospecific formation of dichloride amino oxime derivatives **1a** and **1b** (or **1a'** and **1b'**) or bis-chelating amino oxime oximato compounds **2a** and **2b** (or **2a'** and **2b'**). Coordination of the amino-N to palladium affords new stereogenic centers at the nitrogen atoms, resulting in the formation of different diastereomers. The stereoselectivity of the process strongly depends on the nature of the amino substituents and enables the stereospecific formation of amino oxime oximato compounds **2a** and **2a'** under the reaction conditions used.

The behavior in water of compound **2b** at different pH values was evaluated by NMR spectroscopy. Inversion of the coordinated-N configuration of **2b** takes place in coordinating solvents like water or methanol, where a different ratio of diastereomers than that observed in chloroform is detected. The characterization data collected probe that the mixture of epimers remains unaltered in solution within a pH range of 2.0-12.0. Regarding the biological study, the oxime oximato-containing Pd(II) compounds evaluated have shown high anticancer activities against the cancer cell lines tested. **2a** and especially **2a'** are the most active derivatives, with IC_{50} values up to 80 times better than cisplatin in the PC-3 cell line. In addition, **2a'** shows selective cytotoxicity against tumor cells, with a selectivity index close to 30. Furthermore, both enantiomers show significantly different IC_{50} values. DNA interactions have been studied for **2a**, **2a'**, **2b**, and **2b'** by equilibrium dialysis, DNA melting assays, and viscosity titrations. The results allow concluding that the metal complexes bind CT DNA with moderate affinity, and likely interact with DNA by partial, non-classical intercalation and/or by groove binding. On the other hand, cell cycle assay of PC-3 cells in the presence of enantiomers **2a** and **2a'** reveals cell cycle arrest at the S and G2/M phases, with less affection of the cell distribution in the S-phase compared to cisplatin. This result agrees well with the study of the compound-DNA interactions, which showed weaker structural damage on DNA than that caused by cisplatin.

Experimental section

General considerations

Synthesis of novel palladium complexes was performed without exclusion of moisture or air. (1*S*,4*R*)-, (1*R*,4*S*)-{NOH^NH(R)} (R = Ph **a**, **a'**; Bn **b, b'**) and corresponding adducts (1*S*,4*R*)-, (1*R*,4*S*)-{NOH^NH(R)·HCl} (R = Ph **a·HCl**, **a'·HCl**; Bn **b·HCl**, **b'·HCl**) were prepared from *R*- or *S*-limonene and isopentyl nitrite following the standard method described by Carman et al in 1977.[36,119] *R*-limonene, *S*-limonene, $[Pd(COD)Cl_2]$, $K_2[PdCl_4]$ and cisplatin were purchased from Sigma-Aldrich and used without further purification. NMR spectra were recorded on a Bruker 400 Ultrashield. ^1H and ^{13}C chemical shifts are reported relative to tetramethylsilane and ^{15}N chemical shifts relative to liquid ammonia (25 °C). Compounds' concentrations used were within the range 4-25 mM. Coupling constants J are given in Hertz. Elemental analyses were performed at our laboratories (UAH) on a LECO CHNS-932 analyzer or, alternatively, at the Universidad Autónoma de Madrid on analogous LECO CHNS-932 analyzer. High Resolution Electrospray Ionization Mass Spectroscopy was performed on a Bruker MAXIS II spectrometer. IR spectra were recorded on IR FT Perkin Elmer (Spectrum 2000) spectrophotometer on KBr pellets. The pH was measured in a HANNA HI208 pHmeter in distilled water solutions. Optical rotations of the compounds' solutions were recorded on a Perkin Elmer 341 polarimeter, using the sodium

D line (589 nm) at ambient temperature (297 K) in a quartz cell of 1 dm path length. Specific optical rotation values were calculated according to the equation $[\alpha]^{24}_D = 100\cdot\alpha_{obs}/l\cdot c$.[120] Analytical balance and volumetric pipettes (2.0 mL) were used to prepare $CHCl_3$ solutions of the compounds at concentrations within a range of 4.00-4.50 mg·mL^{-1}. UV spectra were measured at room temperature on water or water PBS (phosphate buffered saline) solutions of the compounds with a Perkin Elmer Lambda 35 spectrophotometer. Phosphate buffered saline solution (PBS) were prepared according to Cold Spring Harbor Protocols (http://cshprotocols.cshlp.org/content/2006/1/pdb.rec8247) using NaCl, KCl, Na_2HPO_4 and KH_2PO_4 in water-d_2.

[Pd{(1*S*,4*R*)-NOH^NH(Ph)-κ²N}Cl₂] and [Pd{(1*R*,4*S*)-NOH^NH(Ph)-κ²N}Cl₂] (1a, 1a').

A dichloromethane (5 mL) solution of (1*S*,4*R*)- or (1*R*,4*S*)-[NOH^NH$_2$(Ph)][Cl] (103 mg, 0.35 mmol) and [Pd(COD)Cl$_2$] (0.10 g, 0.35 mmol) was stirred for 24 hours at room temperature. Solvent, COD and HCl were evaporated to dryness to afford an orange solid, which was washed with methanol and diethylether and dried under vacuum or in an Eppendorf™ Vacufuge™ concentrator.

Yield: 183 mg, 0.29 mmol, 83% (**1a**), 205 mg, 0.33 mmol, 94% (**1a'**). Solubility in H_2O at 24 °C (mM): 0.87 ±0.4 mM. Value of pH ([0.3 mM]) in H_2O at 24 °C: 3.77. Anal. Calcd for $C_{16}H_{22}N_2OPdCl_2$: C, 44.11; H, 5.09; N, 6.43%; Found **1a-1+1a-2**: C, 44.33; H, 5.25; N, 6.38%, **1a1'+1a2'**: C, 44.57; H, 5.19; N, 5.97. FTIR (KBr): ῡ 3432 (OH); 1642 (C=N). NMR spectroscopic data collected allows detection and full assignment of the resonances due to [Pd{(R_N,1*S*,4*R*)-NOH^NH(Ph)-κ²N}Cl$_2$] (**1a-1**) (or [Pd{(S_N,1*R*,4*S*)-NOH^NH(Ph)-κ²N}Cl$_2$] (**1a'-1**)) and [Pd{(S_N,1*S*,4*R*)-NOH^NH(Ph)-κ²N}Cl$_2$] (**1a-2**) (or [Pd{(S_N,1*R*,4*S*)-NOH^NH(Ph)-κ²N}Cl$_2$] (**1a'-2**)), observed in a ratio of ca. 1:0.2. ^{1}H NMR (plus HSQC, plus HMBC, plus COSY, 400.1 MHz, 293 K, $CDCl_3$) **1a-1** or **1a'-1**: δ 9.93 (s, 1H, -NOH), 7.76, 7.37, 7.29 (all m, 5H, -C_6H_5), 6.70 (s, 1H, -NH), 4.97, 4.76 (both s, each 1H, =CH_2), 3.53 (d, J_{HH}=18 Hz, 1H, -CH_2^3), 2.49 (m, 1H, -CH-C=), 2.27 (m, 1H, -CH_2^3), 2.25 (s, 3H, NC-CH_3), 1.85, 1.72 (m, each 1H, -CH_2^5), 1.57 (s, 3H, CH_3C=), 1.44, 1.24 (m, each 1H, CH_2^6). **1a-2** or **1a'-2**: δ 10.07 (s, 1H, -NOH), 7.85-6.83 (all m, 5H, -C_6H_5), 5.59 (s, 1H, -NH), 5.04, 4.84 (both s, each 1H, =CH_2), 3.51 (d, J_{HH}=18 Hz, 1H, -CH_2^3), 2.49 (m, 1H, -CH-C=), 2.21 (m, 1H, -CH_2^3), 2.03 (m, 1H, -CH_2^5), 1.65 (s, 3H, NC-CH_3), 1.56 (m, 1H, -CH_2^6), 1.51 (m, 1H, -CH_2^5), 1.50 (s, 3H, CH_3C=), 1.44 (m, 1H, -CH_2^6). ^{13}C- NMR (plus APT, plus gHSQC, plus HMBC, 100.6 MHz, 293 K, $CDCl_3$) **1a-1** or **1a'-1**: δ 170.5 (+, Cq=N), 144.9 (+, =Cq-Me), 140.9 (+, C_{ipso}Ph), 131.3, 129.5, 128.2, 127.9 (−, C_6H_5), 112.8 (+, =CH_2), 73.5 (+, Cq-NH), 38.0 (−, -CH^4), 30.7 (+, -CH_2^5), 29.6 (−, CH_3-CNH), 29.4 (+, -CH_2^3), 24.9 (+, -CH_2^6), 21.7 (−, *C*H_3-C=). **1a-2** or **1a'-2**: δ 169.0 (+, Cq=N), 144.9 (+, =Cq-Me), 137.9 (+, C_{ipso}Ph), 131.6, 129.5, 128.2, 127.2 (−, C_6H_5), 115.2 (+, =CH_2), 72.4 (+, Cq-NH), 38.8 (−, -CH^4), 32.2 (+, -CH_2^5), 24.2 (−, CH_3-CNH), 28.2 (+, -CH_2^3), 24.6 (+, -CH_2^6), 22.1 (−, *C*H_3-C=). ^{15}N NMR (gHMBC, 40.5 MHz, 293 K, $CDCl_3$): **1a-1** or **1a'-1**: δ 262.4 (C=NOH), 62.1 (NHPh). **1a-2** or **1a'-2:** δ 256.8 (C=NOH), 67.6 (NHPh).

[Pd{(1*S*,4*R*)-NOH^NH(Bn)-κ²N}Cl₂] and [Pd{(1*R*,4*S*)-NOH^NH(Bn)-κ²N}Cl₂] (1b, 1b').

An analogous procedure to that described for the synthesis of **1a** was followed, starting from (1*S*,4*R*)- or (1*R*,4*S*)-[NOH^NH$_2$(Bn)][Cl] (95.0 mg, 0.32 mmol) and [Pd(COD)Cl$_2$] (91 mg, 0.32 mmol). Evaporation of the solvent affords a yellow solid. Yield: 188 mg, 0.29 mmol, 90% (**1b**), 185 mg, 0.28 mmol, 87% (**1b'**). Solubility in H_2O at 24 °C (mM): 1.37. Value of pH ([1.0 mM]) in H_2O at 24 °C: 3.87. Anal.Calcd for $C_{17}H_{24}N_2OPdCl_2$: C, 45.40; H, 5.39; N, 6.23%; Found **1b**: C, 45.81; H, 5.38; N, 5.87%. **1b'**: C, 45.38; H, 5.30; N, 6.08%. FTIR (KBr): ῡ 3388 (OH); 1637 (C=N).

NMR spectroscopic data collected allows full assignment of the resonances due to [Pd{(R_N,1*S*,4*R*)-NOH^NH(Bn)-κ²N}Cl$_2$] (**1b-1**) (or [Pd{(S_N,1*R*,4*S*)-NOH^NH(Bn)-κ²N}Cl$_2$] (**1b'-1**)) and [Pd{(S_N,1*S*,4*R*)-NOH^NH(Bn)-κ²N}Cl$_2$] (**1b-2**) (or [Pd{(S_N,1*R*,4*S*)-NOH^NH(Bn)-κ²N}Cl$_2$] (**1b'-2**)), observed in a ratio of ca. 0.8:1. ^{1}H NMR (plus HSQC, plus HMBC, plus COSY, 400.1 MHz, 293 K, $CDCl_3$) **1b-1** or **1b'-1**: δ 9.79 (s, 1H, -NOH), 7.61, 7.36 (all m, 5H, -C_6H_5), 4.99 (s, 1H, =CH_2), 4.87 (br s, 1H, -NH), 4.73 (dd, J_{HH}=2.3 Hz, J_{HH}=14.6 Hz, 1H, -CH_2-C_6H_5), 4.60 (s, 1H, =CH_2), 4.08 (dd, J_{HH}=8.3 Hz, J_{HH}=14.6 Hz 1H, -CH_2-C_6H_5), 3.32 (d, J_{HH}=17.2 Hz, 1H, -CH_2^3), 2.49 (m, 1H, -CH-C=), 2.18 (m, 1H, -CH_2^3), 2.14 (m, 1H, -CH_2^5), 2.04 (s, 3H, -NC-CH_3), 1.90 (m, 1H, CH_2^6), 1.72 (s, 3H, CH_3C=), 1.63 (m, 1H, CH_2^6), 1.27 (m, 1H, CH_2^5). **1b-2** or **1b'-2**: δ 9.98 (s, 1H, -NOH), 7.52, 7.30 (all m, 5H, -C_6H_5), 5.47 (overlapped, 1H, -NH), 5.09 (dd, J_{HH}=3 Hz, J_{HH}=15 Hz, 1H, -CH_2-C_6H_5), 4.91, 4.68 (both s, each 1H, =CH_2), 3.88 (dd, J_{HH}=9.6 Hz, J_{HH}=15 Hz, 1H, -CH_2-C_6H_5), 3.38 (d, J_{HH}=17.6 Hz, 1H, -CH_2^3), 2.38 (m, 1H, -CH-C=), 2.25 (m, 1H, -CH_2^3), 1.85 (s, 3H, -NC-CH_3), 1.63 (m, 1H, -CH_2^6), 1.60 (s, 3H, CH_3C=), 1.50 (m, 1H, CH_2^6), 1.47 (m, 1H, CH_2^5), 1.10 (m, 1H, CH_2^5). ^{13}C- NMR (plus APT, plus gHSQC, plus HMBC, 100.6 MHz, 293 K, $CDCl_3$): **1b-1** or **1b'-1**: δ 169.1 (+, Cq=N), 145.2 (+, =Cq-Me), 135.9 (+, C_{ipso}Ph), 129.4, 129.2, 129.1, 128.8, 128.5 (−, C_6H_5), 112.5 (+, =CH_2), 71.8 (+, Cq-NH), 52.6 (+, -CH_2Ph), 37.6 (−, -CH^4), 30.0 (+, -CH_2^5), 29.6 (−, *C*H_3-CNH). 29.0 (+, -CH_2^3), 24.5 (+, -CH_2^6), 21.7 (−, *C*H_3-C=). **1b-2** or **1b'-2**: δ 170.3 (+, Cq=N), 143.6 (+, =Cq-Me), 137.1 (+, C_{ipso}Ph), 129.4, 129.2, 129.1, 128.8, 128.6 (−, C_6H_5), 113.1 (+, =CH_2), 71.4 (+, Cq-NH), 55.1 (+, -CH_2Ph), 37.9 (−, -CH^4), 34.5 (+, -CH_2^5), 29.1 (+, -CH_2^3), 24.8 (+, -CH_2^6), 22.9 (−, *C*H_3-CNH), 21.6 (−, *C*H_3-C=). ^{15}N NMR (gHMBC, 40.5 MHz, 293 K, $CDCl_3$): **1b-1** or **1b'-1**: δ 257.2 (C=NOH), 50.9 (NHBn). **1b-2** or **1b'-2**: δ 264.2 (C=NOH), 54.1 (NHBn).

[Pd{(1*S*,4*R*)-NO^NH(Ph)-κ²N}{(1*S*,4*R*)-NOH^NH(Ph)-κ²N}][Cl] and [Pd{(1*R*,4*S*)-NO^NH(Ph)-κ²N}{(1*R*,4*S*)-NOH^NH(Ph)-κ²N}][Cl] (2a, 2a').

A dichloromethane (5 mL) solution of (1*S*,4*R*)- or (1*R*,4*S*)-{NOH^NH(Ph)} (150 mg, 0.56 mmol) and NEt$_3$ (156 µL, 1.12 mmol) was added to a solution of [Pd(COD)Cl$_2$] (80 mg, 0.28 mmol) in dichloromethane (5mL), and the mixture was stirred for 24 hours at room temperature. The resulting green-yellow suspension was evaporated to dryness and extracted with toluene, then filtered to eliminate insoluble [NHEt$_3$]Cl, and the final orange-yellow solution was dried under vacuum to afford

a yellowish solid. Further purification is sometimes needed to eliminate residual [$NHEt_3$]Cl by washing the solid with water (2mL) and diethylether (2 mL) and dried under vacuum or in a Eppendorf™ Vacufuge™ concentrator. Yield: 130.6 mg, 0.19 mmol, 69% (**2a**); 110.0 mg, 0.17 mmol, 61% (**2a'**).

Anal.Calcd for $C_{32}H_{43}N_4O_2PdCl{\cdot}H_2O$ (**2a** or **2a'**): C, 56.89; H, 6.71; N, 8.29%; Found (**2a**): C, 57.16 H, 6.56; N, 7.50%. (**2a'**): C, 57.03; H, 6.56; N, 8.53%. High Resolution Electrospray Ionization Mass Spectrometry (HR-ESI-MS): Evaporation of water solutions of **2a** (or **2a'**) affords samples with the following ESI spectra, **2a**: m/z found (calcd) 621.2419 (621.2428) 100%, **2a':** 621.2431 (621.2428) 100%, $[M\text{-}Cl]^+$. $[\alpha]^{23}_D$ (deg·dm^{-1}·dL·g^{-1}) = 10.35 ± 1.3 **2a**, 10.33 ± 1.3 **2a'**. Solubility in H_2O at 24 °C (mM): 0.5 ± 0.1 mM. Value of pH ([0.3 mM]) in H_2O at 24 °C: 5.00. FTIR (KBr): ῡ 3389 (OH); 1644 (C=N). NMR spectroscopic data in chloroform-d_1 confirmed the presence of a single detectable stereoisomer. ^{1}H NMR (plus HSQC, plus HMBC, plus COSY, 400.1 MHz, 293 K, chloroform-d_1): δ 18.03 (br, 1H, -NOH), 8.77, 8.52 (both s, each 1H, -NH), 7.30-6.70 (m, 10H, $-C_6H_5$), 5.08, 4.95, 4.86, 4.79 (all s, each 1H, $=CH_2$), 3.69 (d, 1H, J_{HH}= 17 Hz, $-CH_2^3$), 3.64 (d, 1H, J_{HH}= 17 Hz, $-CH_2^3$), 2.79 (m, 1H, $-CH_2^6$), 2.63, 2.40 (m, 2H, -CH-C=), 2.25 (m, 2H, $-CH_2^3$), 2.12 (m, 2H, $-CH_2^5$ + $-CH_2^6$), 2.02 (s, 3H, NC-CH_3), 1.90 (m, 1H, $-CH_2^5$), 1.82 (s, 3H, CH_3C=), 1.74 (m, 2H, $-CH_2^5$), 1.50 (s, 3H, CH_3C=), 1.22 (m, 1H, $-CH_2^6$), 1.06 (m, 1H, $-CH_2^6$), 1.00 (s, 3H, NC-CH_3). ^{13}C- NMR (plus APT, plus gHSQC, plus HMBC, 100.6 MHz, 293 K, chloroform-d_1): δ 166.2 (+, C=NO), 162.7 (+, C=NO), 145.2 (+, =C-Me), 144.8 (+, =C-Me), 140.6 (+, $C_{ipso}C_6H_5$), 140.5 (+, $C_{ipso}C_6H_5$), 128.9, 128.7, 128.1, 128.0, 126.7, 126.2, 126.1, 125.7, 124.9, 124.1 (–, C_6H_5), 112.5, 112.1 (+, $=CH_2$), 71.5, 70.6 (+, Cq-NH), 42.3, 38.4 (–, $-CH^4$), 38.2, 30.7 (+, $-CH_2^5$), 29.7 (–, CH_3-CNH), 29.1, 28.9 (+, $-CH_2^3$), 25.8, 25.7 (+, $-CH_2^6$), 22.6 (–, CH_3-C=), 22.3 (–, CH_3-CNH), 21.3 (–, CH_3-C=). ^{15}N NMR (gHMBC, 40.5 MHz, 293 K, chloroform-d_1): δ 276.0, 268.0 (=NOHON=), 68.5, 65.7 (NHPh).

[Pd{(1*S*,4*R*)-NO^NH(Bn)-κ^{2}N}{(1*S*,4*R*)-NOH^NH(Bn)-κ^{2}N}][Cl] and [Pd{(1*R*,4*S*)-NO^NH(Bn)-κ^{2}N}{(1*R*,4*S*)-NOH^NH(Bn)-κ^{2}N}][Cl] (2b, 2b').

A procedure analogous to that used for the synthesis of **2a** (or **2a'**) was followed, starting from (1*S*,4*R*)- or (1*R*,4*S*)-{NOH^NH(Bn)} (190 mg, 0.70 mmol), NEt_3 (195 µL, 1.4 mmol) and [$Pd(COD)Cl_2$] (100 mg, 0.35 mmol). The resulting solid is green-yellow coloured. Yield: 176 mg, 0.27 mmol, 77% (**2b**). 149 mg, 0.23 mmol, 71% (**2b'**).

Anal.Calcd for $C_{34}H_{47}N_4O_2PdCl$: C, 59.56; H, 6.91; N, 8.17%; Found (**2b**): C, 58.99; H, 6.91; N, 7.72%; (**2b'**): C, 59.91; H, 7.05; N, 7.54%. High Resolution Electrospray Ionization Mass Spectrometry (HR-ESI-MS): m/z found (calcd) 649.2749 (649.2741) 100% (**2b**). Solubility in H_2O at 24 °C (mM): 5.8 ± 0.3 mM. Value of pH ([2.0 mM]) in H_2O at 24 °C: 7.33. FT IR (KBr): ῡ 3385 (OH); 1640 (C=N). NMR spectroscopic data in chloroform-d_1 confirmed the presence of two different stereoisomers, **2b-1** + **2b-2** *(*or **2b'-1** + **2b'-2***)*, in ca. 1:0.3 ratio. Some of the resonances of the minor stereoisomer are overlapped with those due to the major one, but many can be assigned by relative integration and bidimensional ^{1}H-^{13}C experiments. ^{1}H NMR (plus HSQC, plus HMBC, plus COSY, 400.1 MHz, 293 K, chloroform-d_1), **2b-1** (or **2b'-1**): δ 18.20 (s, 1H, -NOH), 7.86, 7.40, 7.30 (all m, 10H, $-C_6H_5$), 5.90 (br, 2H, -NH), 5.02, 4.81 (both s, each 2H, $=CH_2$), 4.36, 4.19 (dd, each 2H, J_{HH}= 8 Hz, J_{HH}= 13 Hz, $-CH_2$-C_6H_5), 3.62 (d, 2H, J_{HH}= 18 Hz, $-CH_2^3$), 2.43 (m, 2H, -CH-C=), 2.11 (dd, 2H, J_{HH}= 6 Hz, J_{HH}= 18 Hz, $-CH_2^3$), 1.99 (m, 2H, $-CH_2^6$), 1.88 (m, 2H, $-CH_2^5$), 1.68 (s, 6H, CH_3C=), 1.58 (m, 2H, $-CH_2^5$), 1.35 (m, 2H, $-CH_2^6$), 1.14 (s, 6H, NC-CH_3). **2b-2** (or **2b'-2**): δ 18.32 (s, 1H, -NOH), 7.96, 7.43, 7.27-7.13 (all m, 10H, $-C_6H_5$), 5,90 (overlapped, 1H, NH), 5.58 (br, 1H, -NH), 4.98, 4.87, 4.80, 4.67 (all s, each 1H, $=CH_2$), 4.64, 4.10, 3.78, 2.40 (m, each 1H, $-CH_2$-C_6H_5), 3.62 (overlapped, 1H, $-CH_2^3$), 2.49 (m, 1H, $-CH^4$-C=), 2.32 (s, 3H, NC-CH_3), 2.30 (m, 1H, $-CH^4$-C=), 2.42, 2.31, 1.98, 1.96, 1.78, 1.71, 1.60, 1.53, 1.35, 1.24, 0.77 (m, each 1H, $-CH_2^{3,5,6}$), 1.72, 1.58 (both s, each 3H, CH_3C=), 1.12 (s, 3H, NC-CH_3). ^{13}C-NMR (plus APT, plus gHSQC, plus HMBC, 100.6 MHz, 293 K, chloroform-d_1): **2b-1** (or **2b'-1**) δ 162.2 (+, C=NO), 145.9 (+, =C-Me), 137.9 (+, $C_{ipso}C_6H_5$), 129.6, 129.4, 129.4, 128.5, 128.5 (–, C_6H_5), 122.2 (+, $=CH_2$), 68.6 (+, C-NH), 53.5 (+, $-CH_2$- C_6H_5), 38.6 (–, $-CH^4$), 29.2 (+, $-CH_2^6$), 28.9 (+, $-CH_2^3$), 27.9 (–, CH_3-CNH), 25.5 (+, $-CH_2^5$), 21.9 (–, CH_3-C=). **2b-2** (or **2b'-2**) δ 164.2, 162.7 (+, C=NO), 146.6, 144.3 (+, =C-Me), 137.3, 136.8 (+, $C_{ipso}C_6H_5$), 131.4, 129.8, 129.4, 129.1, 128.8, 128.8, 128.6, 128.3, 128.2, 125.4 (–, C_6H_5), 112.7, 112.1 (+, $=CH_2$), 69.1, 68.8 (+, C-NH), 53.4, 53.2 (+, $-CH_2$-C_6H_5), 39.0, 38.4 (–, $-CH^4$), 35.4, 29.2, 29.0, 28.7, 28.1, 25.6 (+, $-CH_2^{3,5,6}$), 30.9, 21.5 (–, CH_3-CNH), 22.1, 21.8 (–, CH_3-C=). ^{15}N NMR (gHMBC, 40.5 MHz, 293 K, chloroform-d_1): **2b-1** (or **2b'-1**) δ 274.1 (=NOHON=), 51.7 (NHBn). **2b-2** (or **2b'-2**) δ 274.1, 279.0 (=NOHON=), 53.2, 51.7 (NHBn).

When samples of **2b** (or **2b'**) are dissolved in water-d_2, NMR spectra show the presence of two sets of resonances, **2b-1** + **2b-2** *(*or **2b'-1** + **2b'-2***)*, in ca. 0.1:1 ratio. Due to the low overall intensity of the resonances, only data of the major set of signals (**2b-2**, C_1 symmetry) are given: ^{1}H NMR (plus HSQC, plus HMBC, plus COSY, 400.1 MHz, 293 K, water-d_2): δ 7.91, 7.65, 7.40, 7.22 (all m, 10H, $-C_6H_5$), 5.05, 4.90, 4.73, 4.53 (all s, each 1H, $=CH_2$), 4.12, 3.73, 3.47 (m, each 1H, $-CH_2$-C_6H_5), 3.46, 3.40 (m, each 1H, $-CH_2^{3,5,6}$), 2.72 (m, 1H, -CH-C=), 2.52 (m, 2H, $-CH_2$-C_6H_5 + $-CH_2^{3,5,6}$), 2.45 (m, 1H, -CH-C=), 2.34, 2.32 (m, each 1H, $-CH_2^{3,5,6}$), 2.10 (m, 1H, $-CH_2^{3,5,6}$), 1.95 (s, 3H, NC-CH_3), 1.92 (m, 1H, $-CH_2^{3,5,6}$), 1.78 (s, 3H, CH_3C=), 1.59 (+ CH_3C=), 1.58, 1.54, 1.51 (m, each 1H, $-CH_2^{3,5,6}$) 1.22 (m, 1H, $-CH_2^{3,5,6}$), 1.09 (s, 3H, NC-CH_3), 0.91 (m, 1H, $-CH_2^{3,5,6}$). ^{13}C- NMR (plus APT, plus gHSQC, plus HMBC, 100.6 MHz, 293 K, water-d_2): δ 168.8, 165.8 (+, C=NO), 148.1, 147.2 (+, =C-Me), 136.1, 135.2 (+, $C_{ipso}C_6H_5$), 131.7, 131.7, 130.2, 130.1, 130.0, 129.6, 129.5, 129.1, 128.9, 128.7 (–, C_6H_5), 111.2, 110.8 (+, $=CH_2$), 69.0, 69.0 (+, C-NH), 53.2, 51.6 (+, $-CH_2$-C_6H_5), 38.8, 38.1 (–, $-CH^4$), 33.1 (–, $-CH_2^{3,5,6}$), 29.1 (–, *C*H_3-CqNH), 29.0, 28.8, 28.4, 24.9, 24.7 (+, $-CH_2^{3,5,6}$), 21.7 (–, *C*H_3-CqNH), 21.2 (–, *C*H_3-C=), 21.0 (–, *C*H_3-C=). ^{15}N NMR (gHMBC, 40.5 MHz, 293 K, water-d_2): δ 57.5, 49.4 (NHPh), NOH not observed.

When samples of **2b** (or **2b'**) are dissolved in methanol-d_4, NMR spectra show the presence of two sets of resonances, **2b-1** + **2b-2** *(*or **2b'-1** + **2b'-2***)*, in ca. 0.1:1 ratio. Low intensity of the minor set of signals and overlapping in the ^{1}H NMR preclude their full assignment, however, ^{13}C NMR and ^{15}N NMR spectra allows detection of the resonances due to both sets. ^{1}H NMR (plus HSQC, plus HMBC, plus COSY, 400.1 MHz, 293 K, methanol-d_4)

2b-2: δ 7.84 (m, 2H, -C_6H_5), 7.55 (m, 3H, -C_6H_5), 7.25 (m, 3H, -C_6H_5), 7.12 (m, 2H, -C_6H_5), 4.95, 4.78, 4.74, 4.62 (all s, each 1H, =CH_2), 4.02, 3.64, 3.64, 2.36 (m, each 1H, -CH_2Ph), 3.47 (m, 2H, -$CH_2^{3,5,6}$), 2.52, 2.29 (m, each 1H, -CH-C=), 2.22, 2.01 (m, each 1H, -$CH_2^{3,5,6}$), 2.02 (s, 3H, NC-CH_3), 2.03, 1.96, 1.91(m, each 1H, -$CH_2^{3,5,6}$), 1.73 (s, 3H, CH_3C=), 1.54 (s, 3H, CH_3C=), 1.52, 1.46, 1.20, (m, each 1H, -$CH_2^{3,5,6}$), 0.97 (s, 3H, NC-CH_3), 0.62 (m, 1H, -$CH_2^{3,5,6}$). ^{13}C- NMR (plus APT, plus gHSQC, plus HMBC, 100.6 MHz, 293 K, methanol-d_4) **2b-1**: δ 164.2 (+, C=NO), 147.8 (+, =C-Me), 138.4 (+, $C_{ipso}C_6H_5$), 130.5, 130.5, 130.2, 130.2, 129.8 (–, C_6H_5), 111.2 (+, =CH_2), 69.9 (+, Cq-NH), 54.2 (+, -CH_2-Ph), 40.0 (–, -CH^4), 30.2, 29.9, 25.8 (–, -$CH_2^{3,5,6}$), 28.6 (–, *C*H_3-CqNH), 23.4 (–, *C*H_3-C=). **2b-2**: δ 167.0, 163.2 (+, C=NO), 148.4, 146.1 (+, =C-Me), 138.5, 136.9 (+, C_{ipso}Ph), 133.0, 133.0, 130.9, 130.9, 130.6, 130.5, 130.5, 130.0, 130.0, 129.7 (–, C_6H_5), 112.5, 112.3 (+, =CH_2), 69.9, 69.6 (+, C-NH), 54.2, 54.0 (+, -CH_2-Ph), 40.3, 39.8 (–, -CH^4), 35.2, 30.0, 29.6, 29.5, 26.2, 26.0 (+, -$CH_2^{3,5,6}$), 29.8 (–, *C*H_3-CqN), 22.0 (–, *C*H_3-C=), 21.9, 21.9 (–, *C*H_3-CNH + *C*H_3-C=). ^{15}N NMR (gHMBC, 40.5 MHz, 293 K, dmso-d_6) **2b-1**: 270.4 (NOH), 49.2 (NHPh). **2b-2:** 278.3, 267.7 (NOH), 58.6, 47.7 (NHPh).

When samples of **2b** (or **2b'**) are dissolved in DMSO-d_6, NMR spectroscopic data showed one major set of resonances attributable to a C_1 symmetric compound (**2b-2**). Low intensity of the minor set of signals precludes their full assignment, and only those due to 2b-2 are given. ^{1}H NMR (plus HSQC, plus HMBC, plus COSY, 400.1 MHz, 293 K, dmso-d_6): δ 18.45 (s, 1H, -NOH), 7.84, 7.57, 7.31, 7.25 (all m, all 10H, -C_6H_5), 7.05, 6.60 (br, each 1H, -NH), 4.96, 4.82, 4.69, 4.58 (all s, each 1H, =CH_2), 4.02, 3.84, 3.54, 2.07 (m, each 1H, -CH_2Ph), 3.27 (m, 1H, -CH_2^3), 2.52 (m, 1H, -CH-C=), 2.51 (m, 1H, -CH_2^3), 2.50 (m, 1H, -CH_2^6), 2.27 (m, 1H, -CH_2^5), 2.25 (m, 1H, -CH-C=), 2.24 (m, 1H, -CH_2^3), 2.17 (m, 1H, -CH_2^3), 2.12 (s, 3H, NC-CH_3), 2.11 (m, 1H, -CH_2^5), 2.06 (m, 1H, -CH_2-C_6H_5), 1.89 (m, 1H, -CH_2^5), 1.73 (s, 3H, CH_3C=), 1.54 (s, 3H, CH_3C=), 1.51 (m, 1H, -CH_2^6), 1.39 (m, 1H, -CH_2^5), 1.20 (m, 1H, -CH_2^6), 0.97 (s, 3H, NC-CH_3), 0.41 (m, 1H, -CH_2^6). ^{13}C- NMR (plus APT, plus gHSQC, plus HMBC, 100.6 MHz, 293 K, dmso-d_6): δ 163.9, 161.0 (+, C=NO), 146.8, 144.7 (+, =C-Me), 137.2, 135.5 (+, C_{ipso}Ph), 131.4, 131.4, 129.0, 129.0, 128.7, 128.3, 128.3, 128.1, 128.0, 127.9 (–, C_6H_5), 111.4, 110.9 (+, =CH_2), 67.8, 67.6 (+, C-NH), 52.3, 51.9 (+, -CH_2Ph), 38.2, 37.7 (–, -CH^4), 33.5 (–, -CH_2^6), 29.1 (–, *C*H_3-CqNH), 28.4, 28.1 (+, -CH_2^3), 27.9 (+, -CH_2^6), 24.6, 24.5 (+, -CH_2^5), 21.5, 21.2 (–, *C*H_3-C=), 20.7 (–, *C*H_3-CqNH). ^{15}N NMR (gHMBC, 40.5 MHz, 293 K, dmso-d_6): δ 278.3, 265.3 (C=NOH), 57.7, 47.4 (NHPh).

[Pd{(1*S*,4*R*)-NO^NH(Bn)-κ^{2}N}{(1*S*,4*R*)-NOH^NH(Bn)-κ^{2}N}][PF_6] (2b·PF_6).

A dichloromethane (5 mL) solution of **2b** (20 mg, 0.029 mmol) and KPF_6 (5.4 mg, 0.029 mmol) was stirred for 8 hours at 25 °C. The resulting suspension was filtered and dried under vacuum to afford a yellow solid. Yield: 14.0 mg, 0.017 mmol, 59%. ^{1}H NMR spectroscopic data in chloroform-d_1 confirmed the presence of two different isomers, **2b-1·PF_6** + **2b-2·PF_6**, in a 1:0.3 ratio. Data of the major isomer is given: ^{1}H NMR (plus HSQC, plus HMBC, plus COSY, 400.1 MHz, 293 K, chloroform-d_1): δ 18.08 (s, 1H, -NOH), 7.63, 7.45, 7.36 (all m, 10H, -C_6H_5), 5.02, 4.81 (both s, each 2H, =CH_2), 4.18 (m, 2H, -CH_2-C_6H_5), 4.08 (br, 2H, -NH), 4.01 (m, 2H, -CH_2-C_6H_5), 3.65 (d, 2H, J_{HH}= 18 Hz, -CH_2^3), 2.45 (m, 2H, -CH-C=), 2.12 (dd, 2H, J_{HH}= 6 Hz, J_{HH}= 18 Hz, -CH_2^3), 1.97 (m, 4H, -CH_2^6 + -CH_2^5), 1.69 (s, 6H, CH_3C=), 1.61 (m, 2H, -CH_2^5), 1.39 (m, 2H, -CH_2^6), 1.04 (s, 6H, NC-CH_3). ^{19}F NMR (376.5 MHz, 293 K, chloroform-d_1): δ = –70.8 (d, $J_{P,F}$ = 715 Hz, PF_6) ppm. ^{31}P NMR (161.9 MHz, 293 K, chloroform-d_1): δ = –144.0 (sept, $J_{P,F}$ = 715 Hz, PF_6).

X-ray structure determination of 1a-1, 1a'-1, 1b and 2a'. Yellow crystals of **1a-1**·2$CHCl_3$, **1a'-1**·2$CHCl_3$ and **1b** were grown at room temperature by slow evaporation from solutions of the compounds in $CHCl_3$:*n*-hexane (1:1). Colourless crystals of **2a'**·$C_{16}H_{22}N_2O$ were obtained by slow evaporation from a toluene solution of the complex. The crystals were removed from the vial and covered with a layer of a viscous perfluoropolyether (Fomblin®Y). A suitable crystal was selected with the aid of a microscope, mounted on a cryoloop, and immediately placed in the low temperature nitrogen stream of the diffractometer. The intensity data sets were collected at 200 K on a Bruker-Nonius KappaCCD diffractometer equipped with an Oxford Cryostream 700 unit. Crystallographic data for all the complexes are presented in Table S1.

The structures were solved, using the WINGX package,[121] by intrinsic phasing methods (SHELXT),[122] and refined by least-squares against F^2 (SHELXL-2014/7). Compounds **1a-1** and **1a'-1** crystallized with two molecules of chloroform, which were located in the difference Fourier map. These crystals presented disorders for one of the solvent molecules, which were treated by using the PART tool with final values of 61 and 39% both of them. All non-hydrogen atoms were anisotropically refined, whereas all the hydrogen atoms were positioned geometrically and refined by using a riding model. Additionally, in the crystal of **1a-1**·2$CHCl_3$ SADI restraints were employed for the major position of the disordered chloroform molecule (C(101), Cl(14), Cl(15) and Cl(16)).

The asymmetric unit of **1b** was formed by a pair of the epimers **1b-1** and **1b-2**. In this crystallographic study, all non-hydrogen atoms were anisotropically refined. All the hydrogen atoms were positioned geometrically and refined using a riding model, except those linked to nitrogen (H(2) and H(12)), which were found in the difference Fourier map and refined isotropically. Moreover, DFIX constraints were applied to the distances N(1)-H(2) and N(11)-H(12).

Compound **2a'** crystallized with a ligand molecule. All non-hydrogen atoms were anisotropically refined. All hydrogen atoms were positioned geometrically and refined by using the riding model, except those linked to nitrogen (H(2), H(22) and H(42)) and oxygen (H(1) and H(41)), which were also found in the Fourier map and refined isotropically.

Time- and pH-dependant NMR experiments

Palladium compounds were dissolved in 2000 μL of water-d_2 and final pH* (pH* = pHmeter reading in water-d_2) was adjusted to desired values using a solution of DCl (0.01M) or NaOD (0.01 M) in water-d_2, with the help of a HANNA HI208 pHmeter. Time-dependent ^{1}H NMR spectra of 500 μL aliquots of final solutions were carried out.

n-Octanol–Water Partition Coefficients

The n-octanol–water partition coefficient was measured by using the shake-flask method.[88] Distilled water and n-octanol were stirred together for 72 h at 25 °C, to promote saturation of both phases. The solvents were separated and freshly used. Aliquots of stock solutions (150 μM) of **2a** in the n-octanol saturated aqueous phase were added to equal volumes of water-saturated n-octanol and shaken on a mechanical shaker for 1 h. The resultant biphasic solution was centrifuged to separate the layers, and UV/Vis absorption spectra of both solutions were registered in both phases in a Perkin Elmer Lambda 35 UV/Vis spectrophotometer at 284 nm and compared with a calibration curve to obtain the compound concentration of **2a** in both phases. logP was defined as the logarithm of the ratio [Pd]octanol/[Pd]water or [Pt]octanol/[Pt]water, respectively; values reported are the means of three separate experiments.

***In vitro* cell studies**

Cell culture

The human cervical carcinoma cell line HeLa, the human breast adenocarcinoma cell line MCF-7, the human prostate cancer cell lines PC-3 and non-tumorigenic prostate cells line RWPE-1 were obtained from the American Type Culture Collection (Manassas, VA). MCF-7 cells were grown routinely in DMEM (Dulbecco's modified Eagle's medium), RWPE-1 in complete keratinocyte medium containing 50 μg/ml bovine pituitary extract and 5 ng/ml human epidermal growth factor (EGF), and PC-3 and HeLa cells in RPMI-1640 (Roswell Park Memorial Institute), supplemented with 10% fetal bovine serum (FBS), 200 U·mL^{-1} penicillin and 100 μg·mL^{-1} streptomycin (all from Sigma-Aldrich). The culture was performed in a humidified 5% CO_2 environment at 37 °C. After the cells reached 70–80% confluence, they were washed with PBS, detached with 0.25% trypsin/0.2% EDTA and seeded at 30.000–40.000 cells·cm^{-2}. The culture medium was changed every 3 days. Cultures were maintained in a humidified atmosphere of 95% air: 5% CO_2 at 37 °C. Adherent cells were allowed to attach for 48 h prior to addition of compounds.

MTT Toxicity Assays

For toxicity assays, cells (approximately 5 × 10^3 cells mL^{-1}) were seeded in flat-bottom 96-well plates in complete medium. Adherent cells were allowed to attach for 48 h prior to addition of cisplatin or tested compounds. Stock solutions of ammonium-oxime pro-ligand were freshly prepared in 1% of dimethyl sulfoxide (DMSO) in medium, while cisplatin and new compounds were freshly dissolved in corresponding medium. The stock solutions were then diluted in complete medium and used for sequential dilutions to desired concentrations. The final concentration of DMSO in the cell culture medium did not exceed 0.1%. Control groups with and without DMSO (0.1%) were included in the assays. Compounds were then added at different concentrations in quadruplicate. Cells were incubated with compounds for 72 h, and then cell proliferation was determined by the MTT-reduction method. Briefly, 10 μL/well of [3-(4,5-dimethylthiazol-2-yl)-2,5-diphenyltetrazolium bromide] (MTT) (5 mg·mL^{-1} in PBS) was added, and plates were incubated for 3–4 h at 37 °C. After that time, the culture medium was removed, and the purple formazan crystals formed by the mitochondrial dehydrogenase and reductase activity of vital cells were dissolved in DMSO. The optical density, directly proportional to the number of surviving cells, was quantified at 570 nm (background correction at 630 nm) using a multiwell plate reader and the fraction of surviving cells was calculated from the absorbance of untreated control cells. The IC_{50} value indicates the concentration needed to inhibit the biological function of the cells by half and is presented as a mean ± SD of three independent experiments, each comprising four microcultures per concentration level.

Cell cycle arrest assay

PC-3 (2 × 10^5) cells were grown in 6-well plates. After 24 h, the culture medium was removed and replaced with RPMI-1640 medium containing 0% FBS and 1% antibiotic/antimycotic (penicillin/streptomycin/amphotericin B) for 16 h. After that, cells were subjected to the various treatments for 48 h. Then the cells were washed with PBS and detached with 0.25% trypsin/0.2% EDTA. The cells were centrifuged at 500 × g for 5 min at 4°C and the pellets were mixed with ice-cold 70% ethanol and then kept at −20°C for 30 min. After removing the ethanol by centrifugation, the pellets were washed with PBS and centrifuged again. The supernatants were discarded and the pellets suspended in PBS, 0.2 mg/ml RNase A and 20 μg/ml PI before flow cytometry analysis with a MACSQuant® Analyzer 10 Flow Cytometer (Miltenyi Biotech, 9 Bergisch Gladbach, Germany). Results obtained were analysed with the MacsQuantify 2.13.1 program.

Data analysis

Results were subjected to computer-assisted statistical analysis using One-Way Analysis of Variance ANOVA, Bonferroni´s post-test, and Student´s t-test. Data are shown as the means of individual experiments and presented as the mean ± SD (Standard deviation). Differences of $P < 0.05$ were considered to be significantly different from the controls.

DNA interaction studies

Equilibrium Dialysis

Experiments were carried out as previously reported. [66]Duplex DNA from CT DNA (Calf Thymus deoxyribonucleic acid, Activated, Type XV) was purchased from Sigma Aldrich and used as provided. Dialysis membranes (Spectra/Por® molecular porous membrane tubing, MWCO: 3.5–5.0 kDa; 6.4 mm diameter) were purchased from Spectrum Laboratories Inc. (Repligen). Aqueous solutions of surfactant sodium dodecyl sulfate (SDS) (10%) were purchased from Sigma Aldrich. DNA solutions in phosphate buffer (10 mM NaH_2PO4/Na_2HPO_4, pH = 7.2) were prepared at 75 μM monomeric unit (m.u.) concentrations, in bp.

Dialysis bagswere filled with 75 μM (m.u.) of duplex DNA (200 μL each bag) and placed in a beaker containing 225 mL of ca. 4-5 μM solution of the tested compound. The beaker was covered

with parafilm and aluminium foil and allowed to equilibrate during 24 h at room temperature with continuous stirring. Experiments were run in triplicate. Once the dialysis process had been completed, the solutions from each dialysis bag were transferred to Eppendorf tubes and mixed with an aqueous detergent solution (10%) to reach a SDS concentration of 1% (v/v). The concentrations of free compound in the dialysate solution and compound in the dialysis bags were determined by absorbance measurements using the extinction coefficients of the metal complexes and apparent association constants were determined.[110]

DNA FRET melting assays

Experiments were carried out as previously reported, with some modifications.[66] DNA melting assays were performed using a quantitative PCR kit ABI PRISM® 7000 Sequence Detection System (Applied Biosystems) in a 96-well plate format (96-Well Optical MicroAmp® Reaction Plate, Applied Biosystems, Life Technologies Corporation). The oligonucleotide sequence employed in this experiment, F10T (5'-FAM- TAT AGC TA TA /sp18/ TA TA GCT ATA-TAMRA-3') was synthesized, HPLC-purified and desalted by IDT. FAM is 6-carboxyfluorescein and TAMRA is carboxytetramethylrhodamine. The buffer system was: 10 mM sodium cacodylate, 100 mM LiCl, (pH = 7.3).
First, the duplex-forming oligonucleotide was dissolved in water (Biotechnology Performance Certified, BPC grade) and a 50 µM stock solution was prepared, and then diluted to 0.5 µM and mixed with the working buffer (2x) and water (BPC grade). The DNA solution was heated at 90 °C for 10 min, cooled down slowly for 3 h and left at 4 °C overnight. Compounds were dissolved in water and approximately 1 mM stock solutions were prepared. Stock solutions were then diluted with buffer to obtain 50 µM solutions of each compound. In a 96-well microplate, DNA solutions were mixed with solutions of tested compound and buffer to reach a total volume of 50 µL with a F10T concentration of 0.2 µM, and a compound concentration ranging between 1 and 10 µM.
The melting protocol consisted of an incubation for 5 min at 24 °C, followed by a temperature ramp with a heating rate of 1 °C/min. Conversely, the reverse folding process consisted on incubation at 96°C for 5 min, followed by a temperature ramp with a cooling rate of -1 °C/min. Fluorescence values corresponding to the fluorophore FAM at wavelength of 516 nm (after excitation at 492 nm) were collected at each degree of temperature. Afterwards, the fluorescence data were normalized, plotted against temperature (°C) at each compound concentration, and melting temperatures (Tm) values were estimated as $T_{1/2}$.

Viscosity titrations

Experiments were carried out as previously reported. [66]Duplex DNA from CT (Deoxyribonucleic acid, Activated, Type XV) was purchased from Sigma Aldrich and used as provided. 10 mM phosphate buffer (NaH_2PO_4/Na_2HPO_4) pH = 7.2 was used. The viscosity measurements were performed in a Visco System AVS 470 at 25.00 ± 0.01 °C, using a microUbbelohde (K = 0.01) capillary viscometer. 6 mL of DNA solution (0.4 mM in nucleotides) in phosphate buffer were equilibrated for 20 min at 25.00 °C and then 20 flow times were registered. Small aliquots (25–40 µL) of solutions of metal complexes (1.5-1.7 mM) were added to the DNA solution. Before each flow time registration, the solutions were equilibrated for 20 min to 25.00 °C and then 20 flow times were measured. With the averaged time of the different flow time measurements and the viscometer constant, the viscosities (µ) for each point were calculated. The viscosity results were plotted as $(\mu/\mu_0)^{1/3}$, where μ_0 represents the DNA solution viscosity in the absence of the ligand, versus (r), representing the ratio [ligand]/[DNA].

Conflicts of interest

There are no conflicts to declare.

Acknowledgements

Financial support from Ministerio de Ciencia e Innovación (PID2019-108251RB-I00/AEI/10.13039/501100011033), MINECO (CTQ2015-72625-EXP/AEI), Comunidad Autónoma de Madrid (CAM, I3 Program) and the Universidad de Alcalá (UAH, Projects UAH-AE-2017-2, CCG2020/CC-026, CCG2015/BIO-010 and CCG20/CC-007) is acknowledged. I.C.A. and E.T.R. are grateful to UAH and Ministerio de Educación y Ciencia for their fellowships, respectively.

Notes and references

1 L. Kelland, *Nat. Rev. CANCER*, 2007, **7**, 573–584.
2 M. Hanif and C. G. Hartinger, *Future Med. Chem.*, 2018, **10**, 615–617.
3 R. G. Kenny and C. J. Marmion, *Chem. Rev.*, 2019, **119**, 1058–1137.
4 L. Andrezálová and Z. Országhová, *J. Inorg. Biochem.*, 2021, **225**, 111624.
5 A. Khoury, K. M. Deo and J. R. Aldrich-Wright, *J. Inorg. Biochem.*, 2020, **207**, 111070.
6 T. C. Johnstone, K. Suntharalingam and S. J. Lippard, *Chem. Rev.*, 2016, **116**, 3436–3486.
7 C. E. McDevitt, M. V Yglesias, A. M. Mroz, E. C. Sutton, M. C. Yang, C. H. Hendon and V. J. DeRose, *J. Biol. Inorg. Chem.*, 2019, **24**, 899–908.
8 I. A. Riddell, T. C. Johnstone, G. Y. Park and S. J. Lippard, *Chem. Eur. J.*, 2016, **22**, 7574–7581.
9 V. Brabec, O. Hrabina and J. Kasparkova, *Coord. Chem. Rev.*, 2017, **351**, 2–31.
10 A. R. Kapdi and I. J. S. Fairlamb, *Chem. Soc. Rev.*, 2014, **43**, 4751–4777.
11 T. Lazarević, A. Rilak and Ž. D. Bugarčić, *Eur. J. Med. Chem.*, 2017, **142**, 8–31.
12 S. Medici, M. Peana, V. M. Nurchi, J. I. Lachowicz, G. Crisponi and M. A. Zoroddu, *Coord. Chem. Rev.*, 2015, **284**, 329–350.

13 M. Fanelli, M. Formica, V. Fusi, L. Giorgi, M. Micheloni and P. Paoli, *Coord. Chem. Rev.*, 2016, **310**, 41–79.

14 M. Vojtek, M. P. M. Marques, I. M. P. L. V. O. Ferreira, H. Mota-Filipe and C. Diniz, *Drug Discov. Today*, 2019, **24**, 1044–1058.

15 T. Scattolin, V. A. Voloshkin, F. Visentin and S. P. Nolan, *Cell Reports Phys. Sci.*, 2021, **2**, 100446.

16 N. Nayeem and M. Contel, *Chem. Eur. J.*, 2021, **27**, 8891–8917.

17 M. N. Alam and F. Huq, *Coord. Chem. Rev.*, 2016, 316, 36–67.

18 A. R. Azzouzi, S. Lebdai, F. Benzaghou and C. Stief, *World J. Urol.*, 2015, **33**, 937–944.

19 J. J. Wilson and S. J. Lippard, *Chem. Rev.*, 2014, **114**, 4470–4495.

20 M. Trajkovski, E. Morel, F. Hamon, S. Bombard, M.-P. Teulade-Fichou and J. Plavec, *Chem. Eur. J.*, 2015, **21**, 7798–7807.

21 J. E. Reed, A. J. P. White, S. Neidle and R. Vilar, *Dalton Trans.*, 2009, 2558.

22 O. Nováková, J. Malina, J. Kašpárková, A. Halámiková, V. Bernard, F. Intini, G. Natile and V. Brabec, *Chem. – A Eur. J.*, 2009, **15**, 6211–6221.

23 F. Arnesano, A. Pannunzio, M. Coluccia and G. Natile, *Coord. Chem. Rev.*, 2015, **284**, 286–297.

24 S. A. Abramkin, U. Jungwirth, S. M. Valiahdi, C. Dworak, L. Habala, K. Meelich, W. Berger, M. A. Jakupec, C. G. Hartinger, A. A. Nazarov, M. Galanski and B. K. Keppler, *J. Med. Chem.*, 2010, **53**, 7356–7364.

25 D. Talancón, C. López, M. Font-Bardía, T. Calvet, J. Quirante, C. Calvis, R. Messeguer, R. Cortés, M. Cascante, L. Baldomà and J. Badia, *J. Inorg. Biochem.*, 2013, **118**, 1–12.

26 N. S. Ng, M. J. Wu, S. J. Myers and J. R. Aldrich-Wright, *J. Inorg. Biochem.*, 2018, **179**, 97–106.

27 Z. Zhang, C. Li, X. Sun, C. Gao, C. Yu, Q. Liu, L. Bai, Y. Qian, B. Yang, P. Dong and Y. Zhang, *Inorganica Chim. Acta*, 2017, **455**, 166–172.

28 J. Albert, R. Bosque, M. Crespo, J. Granell, C. López, R. Martín, A. González, A. Jayaraman, J. Quirante, C. Calvis, J. Badía, L. Baldomà, M. Font-Bardia, M. Cascante and R. Messeguer, *Dalton Trans.*, 2015, **44**, 13602–13614.

29 F. Liu, S. Gou, F. Chen, L. Fang and J. Zhao, *J. Med. Chem.*, 2015, **58**, 6368–6377.

30 W. Villarreal, L. Colina-Vegas, C. Rodrigues De Oliveira, J. C. Tenorio, J. Ellena, F. C. Gozzo, M. R. Cominetti, A. G. Ferreira, M. A. B. Ferreira, M. Navarro and A. A. Batista, *Inorg. Chem.*, 2015, **54**, 11709–11720.

31 M. Frik, J. Fernández-Gallardo, O. Gonzalo, V. Mangas-Sanjuan, M. González-Alvarez, A. Serrano Del Valle, C. H. Hu, I. González-Alvarez, M. Bermejo, I. Marzo and M. Contel, *J. Med. Chem.*, 2015, **58**, 5825–5841.

32 Y. Wang, H. Huang, Q. Zhang and P. Zhang, *Dalton Trans.*, 2018, **47**, 4017–4026.

33 M. J. Romero and P. J. Sadler, in *Bioorganometallic Chemistry Applications in Drug Discovery, Biocatalsis and Imaging*, eds. G. Jaouen and M. Salmain, Wiley CH-VCH Verlag GmbH, 2015, vol. Chapter 3, pp. 85–115.

34 P. Papadia, A. Barbanente, N. Ditaranto, J. D. Hoeschele, G. Natile, C. Marzano, V. Gandin and N. Margiotta, *Dalton Trans.*, 2021, **50**, 15655–15668.

35 M. S. I. El Alami, M. A. El Amrani, F. Agbossou-Niedercorn, I. Suisse and A. Mortreux, *Chem. - A Eur. J.*, 2015, **21**, 1398–1413.

36 R. M. Carman, P. C. Mathew, G. N. Saraswathi, B. Singaram and J. Verghese, *Aust. J. Chem.*, 1977, **30**, 1323–1335.

37 I. de la Cueva-Alique, S. Sierra, L. Muñoz-Moreno, A. Pérez-Redondo, A. M. Bajo, I. Marzo, L. Gude, T. Cuenca and E. Royo, *J. Inorg. Biochem.*, 2018, **183**, 32–42.

38 I. De La Cueva-Alique, L. Muñoz-Moreno, Y. Benabdelouahab, B. T. Elie, M. A. El Amrani, M. E. G. Mosquera, M. Contel, A. M. Bajo, T. Cuenca and E. Royo, *J. Inorg. Biochem.*, 2016, **156**, 22–34.

39 I. de la Cueva-Alique, S. Sierra, A. Perez-Redondo, I. Marzo, L. Gude, T. Cuenca and E. Royo, *J. Organomet. Chem.*, 2019, **881**, 150–158.

40 Y. Benabdelouahab, L. Muñoz-Moreno, M. Frik, I. de la Cueva-Alique, M. A. El Amrani, M. Contel, A. M. Bajo, T. Cuenca and E. Royo, *Eur. J. Inorg. Chem.*, 2015, **13**, 2295–2307.

41 C. Bartel, A. K. Bytzek, Y. Y. Scaffidi-Domianello, G. Grabmann, M. A. Jakupec, C. G. Hartinger, M. Galanski and B. K. Keppler, *J. Biol. Inorg. Chem.*, 2012, **17**, 465–474.

42 D. S. Bolotin, M. Y. Demakova, A. A. Legin, V. V. Suslonov, A. A. Nazarov, M. A. Jakupec, B. K. Keppler and V. Y. Kukushkin, *New J. Chem.*, 2017, **41**, 6840–6848.

43 D. B. Dell'Amico, M. Colalillo, L. Dalla Via, M. Dell'Acqua, A. N. Garcia-Argaez, M. Hyeraci, L. Labella, F. Marchetti and S. Samaritani, *Eur. J. Inorg. Chem.*, 2018, 1589–1594.

44 Y. Y. Scaffidi-Domianello, A. A. Legin, M. A. Jakupec, A. Roller, V. Y. Kukushkin, M. Galanski, B. K. Keppie and B. K. Keppler, *Inorg. Chem.*, 2012, **51**, 7153–7163.

45 A. G. Quiroga, L. Cubo, E. de Blas, P. Aller and C. Navarro-Ranninger, *J. Inorg. Biochem.*, 2007, **101**, 104–110.

46 M. Hyeraci, M. Colalillo, L. Labella, F. Marchetti, S. Samaritani, V. Scalcon, M. P. Rigobello and L. Dalla Via, *ChemMedChem*, 2020, **15**, 1464–1472.

47 K. Sayin and D. Karakas, *Spectrochim. ACTA PART A-MOLECULAR Biomol. Spectrosc.*, 2018, **188**, 537–546.

48 N. Bandyopadhyay, P. Basu, G. S. Kumar, B. Guhathakurta, P. Singh and J. P. Naskar, *J. Photochem. Photobiol. B-Biology*, 2017, **173**, 560–570.

49 K. Karami, Z. M. Lighvan, A. M. Alizadeh, M. Poshteh-Shirani, T. Khayamian and J. Lipkowski, *RSC Adv.*, 2016, **6**, 78424–78435.

50 S. Samiee, A. Shiralinia, E. Hoveizi and R. W. Gable, *Appl. Organomet. Chem.*, , DOI:10.1002/aoc.5098.

51 M. M. El-bendary, T. S. Saleh and A. S. Al-Bogami, *Polyhedron*, 2021, **194**, 114924.

52 S. Wirth, C. J. Rohbogner, M. Cieslak, J. Kazmierczak-Baranska, S. Donevski, B. Nawrot and I. P. Lorenz, *J. Biol. Inorg. Chem.*, 2010, **15**, 429–440.

53 S. Adhikari, N. R. Palepu, D. Sutradhar, S. L. Shepherd, R. M. Phillips, W. Kaminsky, A. K. Chandra and M. R. Kollipara, *J. Organomet. Chem.*, 2016, **820**, 70–81.

54 N. R. Palepu, S. Adhikari, R. P. J, A. K. Verma, S. L. Shepherd, R. M. Phillips, W. Kaminsky and M. R. Kollipara, *Appl. Organomet. Chem.*, 2017, **31**, 1–10.

55 N. Chitrapriya, V. Mahalingam, M. Zeller, H. Lee and K. Natarajan, *J. Mol. Struct.*, 2010, **984**, 30–38.

56 N. Chitrapriya, V. Mahalingam, L. C. Channels, M. Zeller, F. R. Fronczek and K. Natarajan, *Inorganica Chim. Acta*, 2008, **361**, 2841–2850.

57 M. Trivedi, S. K. Singh, D. S. Pandey, R. Q. Zou, M. Chandra and Q. Xu, *J. Mol. Struct.*, 2008, **886**, 136–143.

58 Y. H. He, H. Y. Xue, W. D. Zhang, L. Wang, G. Y. Xiang, L. Li and X. M. Shang, *J. Organomet. Chem.*, 2017, **842**, 82–92.

59 L. Menéndez-Rodríguez, E. Tomás-Mendivil, J. Francos, C. Nájera, P. Crochet and V. Cadierno, *Catal. Sci. Technol.*, 2015, **5**, 3754–3761.

60 D. S. Bolotin, N. A. Bokach and V. Y. Kukushkin, *Coord. Chem. Rev.*, 2016, **313**, 62–93.

61 K. Karami, Z. M. Lighvan, S. A. Barzani, A. Y. Faal, M. Poshteh-Shirani, T. Khayamian, V. Eigner and M. Dusek, *NEW J. Chem.*, 2015, **39**, 8708–8719.

62 J. Vicente, M. T. Chicote, A. Abellán-López and D. Bautista, *Dalton Trans.*, 2012, **41**, 752–762.

63 A. Audhya, K. Bhattacharya, M. Maity and M. Chaudhury, *Inorg. Chem.*, 2010, **49**, 5009–5015.

64 I. De La Cueva-Alique, L. Munõz-Moreno, E. De La Torre-Rubio, A. M. Bajo, L. Gude, T. Cuenca and E. Royo, *Dalton Trans.*, 2019, **48**, 14279–14293.

65 E. Abele, R. Abele, L. Golomba, J. Višņevska, T. Beresneva, K. Rubina and E. Lukevics, *Chem. Heterocycl. Compd.*, 2010, **46**, 905–930.

66 S. Soga, L. M. Neckers, T. W. Schulte, Y. Shiotsu, K. Akasaka, H. Narumi, T. Agatsuma, Y. Ikuina, C. Murakata, T. Tamaoki and S. Akinaga, *Cancer Res.*, 1999, **59**, 2931–2938.

67 M. A. Motaleb and A. A. Selim, *Bioorg. Chem.*, 2019, **82**, 145–155.

68 Y. T. Wang, Y. J. Qin, Y. L. Zhang, Y. J. Li, B. Rao, Y. Q. Zhang, M. R. Yang, A. Q. Jiang, J. L. Qi and H. L. Zhu, *RSC Adv.*, 2014, **4**, 32263–32275.

69 N. P. Farrell, *Chem. Soc. Rev.*, 2015, **44**, 8773–8785.

70 S. V. Larionov, T. E. Kokina, L. I. Myachina, L. A. Glinskaya, M. I. Rakhmanova, D. Y. Naumov, A. V. Tkachev and A. M. Agafontsev, *Russ. J. Coord. Chem.*, 2015, **41**, 162–168.

71 N. Bandyopadhyay, M. Zhu, L. Lu, D. Mitra, M. Das, P. Das, A. Samanta and J. P. Naskar, *Eur. J. Med. Chem.*, 2015, **89**, 59–66.

72 N. Bandyopadhyay, M. Das, A. Samanta, M. Zhu, L. Lu and J. P. Naskar, *Chemistryselect*, 2017, **2**, 230–240.

73 A. E. Sorochinsky, H. Ueki, J. L. Aceña, T. K. Ellis, H. Moriwaki, T. Sato and V. A. Soloshonok, *J. Fluor. Chem.*, 2013, **152**, 114–118.

74 H. Mei, M. Jean, M. Albalat, N. Vanthuyne, C. Roussel, H. Moriwaki, Z. Yin, J. Han and V. A. Soloshonok, *Chirality*, 2019, **31**, 401–409.

75 J. W. Faller, B. P. Patel, M. A. Albrizzio and M. Curtis, *Organometallics*, 1999, **18**, 3096–3104.

76 J. W. Faller and N. Sarantopoulos, *Organometallics*, 2004, **23**, 2008–2014.

77 H. Goto, T. Hayakawa, K. Furutachi, H. Sugimoto and S. Inoue, *Inorg. Chem.*, 2012, **51**, 4134–4142.

78 K. Ha, *Acta Crystallogr. E: Structure Reports Online*, 2012, **68**, M176-U894.

79 V. A. Soloshonok, T. K. Ellis, H. Ueki and T. Ono, *J. Am. Chem. Soc.*, 2009, **131**, 7208–7209.

80 A. E. Sorochinsky, H. Ueki, J. L. Aceña, T. K. Ellis, H. Moriwaki, T. Sato and V. A. Soloshonok, *Org. Biomol. Chem.*, 2013, **11**, 4503–4507.

81 M. Munakata, S. Kitagawa and M. Miyazima, *Inorg. Chem.*, 1985, **24**, 1638–1643.

82 T. S. Morais, F. C. Santos, T. F. Jorge, L. Côrte-Real, P. J. A. Madeira, F. Marques, M. P. Robalo, A. Matos, I. Santos and M. H. Garcia, *J. Inorg. Biochem.*, 2014, **130**, 1–14.

83 F. Aman, M. Hanif, W. A. Siddiqui, A. Ashraf, L. K. Filak, J. Reynisson, T. Söhnel, S. M. F. Jamieson and C. G. Hartinger, *Organometallics*, 2014, **33**, 5546–5553.

84 H. P. Varbanov, S. Göschl, P. Heffeter, S. Theiner, A. Roller, F. Jensen, M. A. Jakupec, W. Berger, M. Galanski and B. K. Keppler, *J. Med. Chem.*, 2014, **57**, 6751–6764.

85 A. R. Ghezzi, M. Aceto, C. Cassino, E. Gabano and D. Osella, *J. Inorg. Biochem.*, 2004, **98**, 73–78.

86 J. A. Platts, S. P. Oldfield, M. M. Reif, A. Palmucci, E. Gabano and D. Osella, *J. Inorg. Biochem.*, 2006, **100**, 1199–1207.

87 I. V. Tetko, I. Jaroszewicz, J. A. Platts and J. Kuduk-Jaworska, *J. Inorg. Biochem.*, 2008, **102**, 1424–1437.

88 K. Takács-Novák, A. Avdeef, K. J. Box, B. Podányi and G. Szász, *J. Pharm. Biomed. Anal.*, 1994, **12**, 1369–1377.

89 S. Cruz, S. Bernès, P. Sharma, R. Vazquez, G. Hernández, R. Portillo and R. Gutiérrez, *Appl. Organomet. Chem.*, 2010, **24**, 8–11.

90 A. S. Abu-Surrah, M. Kettunen, M. Leskelä and Y. Al-Abed, *Zeitschrift fur Anorg. und Allg. Chemie*, 2008, **634**, 2655–2658.

91 T. V. Segapelo, S. Lillywhite, E. Nordlander, M. Haukka and J. Darkwa, *Polyhedron*, 2012, **36**, 97–103.

92 D. Gutiérrez, S. Bernès, G. Hernández, O. Portillo, G. E. Moreno, M. Sharma, P. Sharma and R. Gutiérrez, *J. Coord. Chem.*, 2015, **68**, 3805–3813.

93 D. Ning, Y. Cao, Y. Zhang, L. Xia and G. Zhao, *Inorg. Chem. Commun.*, 2015, **58**, 57–59.

94 N. Kordestani, H. Amiri Rudbari, I. Correia, A. Valente, L. Côrte-Real, M. K. Islam, N. Micale, J. D. Braun, D. E. Herbert, N. Tumanov, J. Wouters and M. Enamullah, *New J. Chem.*, 2021, **45**, 9163–9180.

95 A. A. Shabana, I. S. Butler, A. Castonguay, M. Mostafa, B. J. Jean-Claude and S. I. Mostafa, *Polyhedron*, 2018, **154**, 156–172.

96 A. Kumar, A. Naaz, A. P. Prakasham, M. K. Gangwar, R. J. Butcher, D. Panda and P. Ghosh, *ACS Omega*, 2017, **2**, 4632–4646.

97 M. N. Alam and F. Huq, *Coord. Chem. Rev.*, 2016, **316**, 36–67.

98 K. Karami, Z. M. Lighvan, H. Farrokhpour, M. D. Jahromi and A. A. Momtazi-borojeni, *J. Biomol. Struct. Dyn.*, 2018, **36**, 3324–3340.

99 S. G. Churusova, D. V Aleksanyan, E. Y. Rybalkina, O. Y. Susova, A. S. Peregudov, V. V Brunova, E. I. Gutsul, Z. S. Klemenkova, Y. V Nelyubina, V. N. Glushko and V. A. Kozlov, *Inorg. Chem.*, 2021, **60**, 9880–9898.

100 T. T. H. Fong, C. N. Lok, C. Y. S. Chung, Y. M. E. Fung, P. K. Chow, P. K. Wan and C. M. Che, *Angew. Chemie - Int. Ed.*, 2016, **55**, 11935–11939.

101 V. Y. Kukushkin, V. K. Belsky, E. A. Aleksandrova, V. E. Konovalov and G. A. Kirakosyanl, *Inorg. Chem.*, 1992, **31**, 3836–3840.

102 D. V Aleksanyan, S. G. Churusova, Z. S. Klemenkova, R. R. Aysin, E. Y. Rybalkina, Y. V Nelyubina, O. I. Artyushin, A. S. Peregudov and V. A. Kozlov, *Organometallics*, 2019, **38**, 1062–1080.

103 J. Albert, J. Granell, R. Qadir, J. Quirante, C. Calvis, R. Messeguer, J. Badia, L. Baldoma, M. Font-Bardia and T. Calvet, *Organometallics*, 2014, **33**, 7284–7292.

104 M. Alinaghi, K. Karami, A. Shahpiri, A. K. Nasab, A. A. Momtazi-Borojeni, E. Abdollahi and J. Lipkowski, *J. Mol. Struct.*, 2020, **1219**, 128479.

105 H. Skoupilova, R. Hrstka and M. Bartosik, *Med. Chem. (Los. Angeles).*, 2017, **13**, 334–344.

106 F. Ari, B. Cevatemre, E. I. I. Armutak, N. Aztopal, V. T. Yilmaz and E. Ulukaya, *Bioorg. Med. Chem.*, 2014, **22**, 4948–4954.

107 E. Ulukaya, F. Ari, K. Dimas, M. Sarimahmut, E. Guney, N. Sakellaridis and V. T. Yilmaz, *J. Cancer Res. Clin. Oncol.*, 2011, **137**, 1425–1434.

108 D. Kovala-Demertzi, A. Boccarelli, M. A. Demertzis and M. Coluccia, *Chemotherapy*, 2007, **53**, 148–152.

109 C. Cullinane, G. B. Deacon, P. R. Drago, A. P. Erven, P. C. Junk, J. Luu, G. Meyer, S. Schmitz, I. Ott, J. Schur, L. K. Webster and A. Klein, *Dalton Trans.*, 2018, **47**, 1918–1932.

110 J. B. Chaires, in *DNA Binders and Related Subjects*, eds. M. J. Waring and J. B. Chaires, Springer-Verlag Berlin, Berlin, 2005, vol. 253, pp. 33–53.

111 D. Renciuk, J. Zhou, L. Beaurepaire, A. Guedin, A. Bourdoncle and J. L. Mergny, *Methods*, 2012, **57**, 122–128.

112 R. Kieltyka, P. Englebienne, J. Fakhoury, C. Autexier, N. Moitessier and H. F. Sleiman, *J. Am. Chem. Soc.*, 2008, **130**, 10040–10041.

113 D. Suh and J. B. Chaires, *Bioorg. Med. Chem.*, 1995, **3**, 723–728.

114 G. Cohen and H. Eisenberg, *Biopolymers*, 1969, **8**, 45–55.

115 T. A. Fairley, R. R. Tidwell, I. Donkor, N. A. Naiman, K. A. Ohemeng, R. J. Lombardy, J. A. Bentley and M. Cory, *J. Med. Chem.*, 1993, **36**, 1746—1753.

116 N. Sohrabi, N. Rasouli and M. Kamkar, *Bull. Korean Chem. Soc.*, 2014, **35**, 2523–2528.

117 G. Yang, J. Z. Wu, L. Wang, L. N. Ji and X. Tian, *J. Inorg. Biochem.*, 1997, **66**, 141–144.

118 L.-F. Tan and H. Chao, *Inorganica Chim. Acta*, 2007, **360**, 2016–2022.

119 D. Brecknell, R. Carman, B. Singaram and J. Verghese, *Aust. J. Chem.*, 1977, **30**, 195.

120 G. E. Tranter, in *Comprehensive Chirality*, Elsevier Ltd., 2012, vol. 8, pp. 411–421.

121 L. J. Farrugia, *J. Appl. Crystallogr.*, 2012, **45**, 849–854.

122 G. M. Sheldrick, *Acta Crystallogr. C Struct. Chem.*, 2015, **71**, 3–8.